Interrelation between the stability of extended normal modes and the existence of intrinsic localized modes in nonlinear lattices with realistic potentials

K. W. Sandusky and J. B. Page
Department of Physics and Astronomy, Arizona State University, Tempe, Arizona 85287-1504
(Received 12 January 1994)

Previous theoretical studies and molecular dynamics simulations indicate that the anharmonic version of a zone-boundary-mode phonon in a periodic one-dimensional lattice with nearest-neighbor quartic and quadratic interactions is unstable, and that this instability can lead to the production of intrinsic localized modes. We show here that such an instability occurs when nearest-neighbor cubic anharmonicity is added, but that the zone boundary mode is stabilized when the cubic anharmonicity becomes sufficiently large. A direct connection is established between the existence of this instability and the existence of intrinsic localized modes. Furthermore, our analysis reveals the existence of a second type of zone-boundary-mode instability, which is *not* related to intrinsic localized modes. This "period-doubling" instability is also found to occur in one-dimensional lattices with realistic potentials, such as Lennard-Jones, Morse, and Born-Mayer, whereas the instability related to intrinsic localized modes does not occur for these potentials, owing to their inclusion of higher-order anharmonicity. Likewise, intrinsic localized modes are not found in direct numerical searches for these cases, and we conclude that they do not exist in monatomic lattices with these potentials.

I. INTRODUCTION

Recent analytical work and molecular-dynamics simulations confirm that intrinsic localized modes (ILM's) with frequencies above the maximum harmonic frequency and displacements restricted to a few sites exist in nonlinear periodic monatomic one-dimensional lattices with harmonic and quartic nearest-neighbor interactions.[1-13] However, there has been little discussion as to how these modes might be created. Recently, analytical and molecular-dynamics results indicate that an anharmonic version of the harmonic zone-boundary phonon mode (ZBM) in these lattices can decay into one or more ILM's and that an instability for the anharmonic ZBM is the first step in the decay.[14-16] Furthermore, a similar instability exists for a different anharmonic extended phonon mode in lattices having only harmonic intersite coupling, but with realistic nonlinear *on-site* potentials, and this instability can also lead to the production of ILM's.[17,18] In both of these cases, an instability for an extended anharmonic mode appears to play a crucial role in the creation of ILM's. Hence it is important to examine the stability of the ZBM in a nonlinear monatomic lattice with *realistic intersite* potentials that include cubic as well as quartic and harmonic nearest-neighbor interactions.

Stationary modes in homogeneous anharmonic lattices were studied nearly 20 years ago by Kosevich and Kovalev,[19] for lattices with cubic and quartic on-site and intersite anharmonicity. These authors obtained solutions for weakly anharmonic envelope solitons whose spatial extent is broad compared with the lattice spacing. Recently, solutions have been found for very anharmonic, highly localized ILM's which are not described by these envelope soliton solutions (although the latter are recovered for sufficiently weak anharmonicity). For lattices with nearest-neighbor harmonic plus quartic (but no cubic) interactions, the most localized versions of the stationary ILM's are an odd-parity mode $A(\ldots,0,-\frac{1}{2},1,-\frac{1}{2},0,\ldots)$ (Refs. 1 and 2) and an even-parity mode $A(\ldots,0,-\frac{1}{6},1,-1,\frac{1}{6},0,\ldots)$ (Refs. 1 and 4), where A is the mode amplitude.[20] For positive anharmonicity, both of these modes have frequencies well above the maximum harmonic frequency. Furthermore, we showed in a previous paper that the odd-parity mode is unstable against infinitesimal perturbations, while the even mode is stable. However, the instability does *not* destroy the odd-parity ILM; rather, it causes it to move.[13] Figure 1 compares the displacement patterns for these two localized modes with the ZBM displacement pattern. All three modes share the basic "optic-mode" characteristic that adjacent particles vibrate out of phase. Beyond this, these displacement patterns do not suggest any obvious connection between the ZBM and ILM's. However, in an *infinite* harmonic plus quartic lattice, the displacement patterns for both the even- and odd-parity ILM's broaden as the anharmonicity decreases,[21] until they each merge with the ZBM in the harmonic limit.[11,12] A second suggestive feature of the relation between the ILM's and ZBM is revealed by recent analytic studies of a simple four-particle lattice with nearest-neighbor harmonic plus quartic anharmonic interactions and *periodic* boundary conditions.[22] It was shown in these papers that the even- and odd-parity ILM's for this case not only broaden with decreasing anharmonicity, but that both modes merge with the ZBM for a *nonzero* value of the anharmonicity. Moreover, no ILM's were found for anharmonicities below this value. References 22 also gave a stability analysis of the ZBM for this four-particle lattice that revealed another interesting connection: The ZBM first becomes unstable for the same anharmonicity

0163-1829/94/50(2)/866(22)/$06.00

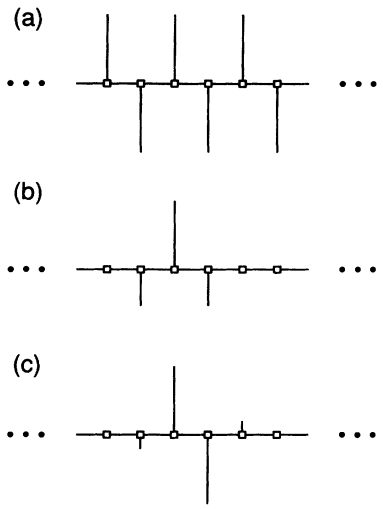

FIG. 1. Predicted displacement patterns for (a) the ZBM, (b) the odd-parity ILM, and (c) the even-parity ILM in a nearest-neighbor harmonic plus quartic lattice in the pure quartic limit. The displacements are measured from the edges of the squares, and they are plotted in the vertical direction for clarity; the physical displacements are actually longitudinal. The odd- and even-parity ILM displacement patterns spread out as the anharmonicity decreases, and for an infinite lattice they merge with the ZBM in the harmonic limit, as discussed in the text. The ZBM pattern is independent of the anharmonicity.

where both of the ILM displacement patterns merge with the ZBM pattern, and the ZBM remains unstable for all anharmonicities greater than this. Hence, in this particular case, the ILM's for a given anharmonicity are predicted to exist if and only if the ZBM for the same anharmonicity is unstable.

It has been shown analytically and confirmed by molecular-dynamics (MD) simulations that ILM's can also exist in lattices with nearest-neighbor *cubic* anharmonicity added to the harmonic and quartic nearest-neighbor interactions.[23,24] In the work to be presented here, we establish firm links between ILM's and the ZBM stability for these more general lattices, similar to the links described above for harmonic plus quartic lattices. In Sec. II A we develop a theory for the stability of stationary anharmonic modes based upon time averages of the equations of motion. This theory is then applied to the ZBM in Secs. II B and II C. We show that while the ZBM is *always* unstable for an infinite harmonic plus quartic lattice, the addition of a sufficiently strong cubic anharmonicity will in fact stabilize the ZBM. These predictions are then confirmed by MD simulations. In Sec. III we show that the anharmonicity thresholds for ILM existence match the ZBM instability thresholds for a wide variety of lattices with nearest-neighbor cubic anharmonicity included. In Sec. IV a different *exact* stability method based upon Floquet's theorem is developed for the ZBM. This method confirms our earlier results based upon the time-averaging approximations, and more importantly, it reveals the existence of new ZBM instabilities not related to the ILM's. In particular, a new ZBM "period-doubling" instability occurs for lattices with strong cubic interactions. Our Floquet ZBM stability analysis is easily generalized to treat lattices with full realistic potentials, such as Lennard-Jones, Morse, and Born-Mayer, and this is done in Sec. IV C. No ZBM instabilities related to the ILM's are found for these potentials. Because of this absence of an ILM-related instability, together with the fact that we do not find ILM's for these potentials in direct numerical searches, we conclude that ILM's do not exist in these lattices, owing to the presence of higher-order anharmonicities in the realistic potentials. Although the ILM's do not exist in monatomic lattices with these realistic intersite potentials, the insights and methods presented here will be very helpful for determining existence criteria for other systems where ILM's *are* found, such as in one-dimensional monatomic lattices with realistic *on-site* potentials[18] and within the phonon gap for one-dimensional *diatomic* lattices with realistic intersite potentials.[25] We further show in Sec. IV C that the new period-doubling ZBM instability found for lattices with strong cubic anharmonicity also occurs in Lennard-Jones, Morse, and Born-Mayer lattices. Section V concludes the paper, and the Appendix provides details on our Floquet-based stability analysis.

II. ROTATING-WAVE-APPROXIMATION STABILITY ANALYSIS

A. Theory

The potential energy for a one-dimensional periodic lattice with harmonic, cubic, and quartic nearest-neighbor interactions is

$$V=\frac{k_2}{2}\sum_n (u_{n+1}-u_n)^2+\frac{k_3}{3}\sum_n (u_{n+1}-u_n)^3 + \frac{k_4}{4}\sum_n (u_{n+1}-u_n)^4 , \quad (1)$$

where k_2, k_3, and k_4 are the harmonic, cubic, and quartic spring constants, respectively, and u_n is the displacement of the nth particle from its equilibrium position. For a purely harmonic lattice, the solutions of the equations of motion are plane waves $u_n=u_0\exp\{i[\omega(k)t-nka]\}$, where a is the equilibrium lattice spacing, and the familiar dispersion relation is $\omega(k)=2\sqrt{k_2/m}\,\sin(ka/2)$. We are interested here in the ZBM, which occurs for $ka=\pi$; in the harmonic approximation, the time-dependent displacements for this mode are $u_n=(-1)^n A\cos(\omega_m t+\phi)$, where A is the mode amplitude, ϕ is an arbitrary constant phase, and the mode frequency $\omega_m=2\sqrt{k_2/m}$ is the maximum harmonic frequency. An anharmonic ZBM with the same $(-1)^n$ displacement pattern also exists in a 1D lattice of particles interacting via the full potential given by Eq. (1). To show this, we substitute a trial solution of the form $u_n=(-1)^n A f(t)$ into the equations of motion, obtaining

$$\ddot{f}=-4\frac{k_2}{m}f-16\frac{k_4 A^2}{m}f^3 , \quad (2)$$

independent of the site index n. Here the $\cos(\omega_m t+\phi)$ time dependence of the harmonic solution has been replaced by a general time-dependent function $f(t)$, with $|f(t)|=1$ when $\dot{f}(t)=0$. This normalization is imposed so that the amplitude A gives the absolute value of the displacements at the anharmonic ZBM turning points. Note that the cubic anharmonicity is absent from Eq. (2); indeed, for a general nearest-neighbor potential, *all* of the odd-order terms in the Taylor-series expansion of the potential drop out of the anharmonic ZBM equations of motion, due to the odd-parity symmetry of the ZBM oscillations about each equilibrium site.

An approximate solution of Eq. (2) is found by substituting $\cos(\omega t)$ for $f(t)$ and making the "rotating-wave approximation" (RWA),[2] in which we identically write

$$\cos^3(\omega t)\equiv\tfrac{3}{4}\cos(\omega t)+\tfrac{1}{4}\cos(3\omega t)$$

and keep just the $\cos(\omega t)$ term. This is equivalent to making the substitution $f(t)\rightarrow\cos(\omega t)$ in Eq. (2), multiplying by $\cos(\omega t)$, and time averaging the resulting equation over the mode period $\tau=2\pi/\omega$. Doing this yields

$$\omega^2/\omega_m^2=1+3\Lambda_4\ , \tag{3}$$

where we have defined the dimensionless quartic anharmonicity parameter $\Lambda_4\equiv k_4A^2/k_2$. For standard potentials such as Lennard-Jones, $\Lambda_4>0$ for physically realistic nearest-neighbor equilibrium separations, and hence the anharmonic ZBM frequency lies above the maximum harmonic frequency ω_m.

The RWA is simple and accurate: The exact ZBM time dependence $f(t)$ determined by Eq. (2) can be obtained in terms of Jacobi elliptic functions,[26] and for the special case $k_2=0$ of purely quartic interactions, the predicted RWA ZBM period differs from the exact result by 2%. Moreover, this difference decreases when harmonic interactions are included. Motivated by this success of the RWA, we now develop a theory for studying ZBM instabilities based upon a time-averaging method which is very similar to that discussed above for the RWA. This method is more analytically tractable than the exact Floquet stability analysis to be presented in Sec. IV and will provide us with a useful analytical expression for the ZBM stability criterion for (k_2,k_3,k_4) lattices.

We will eventually need the equations determining ILM's in general lattices with nearest-neighbor harmonic, cubic, and quartic interactions, together with the linearized equations for infinitesimal ZBM perturbations. Hence the following derivation of the ZBM stability equations will be kept general enough that the ILM equations will also be determined along the way. The derivation is analogous to our derivation of the stability equations for ILM's in harmonic plus quartic lattices in Ref. 13. Here we assume a trial solution of the form

$$u_n(t)=A\xi_n(t)\cos[\omega t+\phi_n(t)]+A\Delta_n(t)\ ,$$

where time- and site-dependent "static" displacements $\{\Delta_n(t)\}$ have now been added to the time- and site-dependent displacements $\{\xi_n\}$ and phases $\{\phi_n\}$ used in Ref. 13. For the ILM's and ZBM, the $\{\Delta_n\}$ are in fact independent of the time, whereas with instability perturbations present they acquire an additional time-dependent part, as will be seen. Their inclusion is essential for lattices with nonzero odd-order anharmonicity. We next assume that the quantities $\{\Delta_n\}$, $\{\xi_n\}$, and $\{\phi_n\}$ all vary slowly on the time scale of the unperturbed mode period, this being consistent with the evolution of both the ZBM instability reported in Ref. 15 for (k_2,k_4) lattices and the ILM instability we studied for the same lattices in Ref. 13. Substituting the trial solution into the equations of motion and time averaging the resulting equation over a mode period, we obtain

$$\begin{aligned}\ddot{\Delta}_n=&\frac{k_2}{m}(\Delta_{n+1}+\Delta_{n-1}-2\Delta_n)+\frac{k_3A}{m}[(\Delta_{n+1}-\Delta_n)^2-(\Delta_{n-1}-\Delta_n)^2]\\&+\frac{k_3A}{2m}[\xi_{n+1}^2-2\xi_{n+1}\xi_n\cos(\phi_{n+1}-\phi_n)+\xi_n^2-\xi_{n-1}^2+2\xi_{n-1}\xi_n\cos(\phi_{n-1}-\phi_n)-\xi_n^2]\\&+\frac{k_4A^2}{m}[(\Delta_{n+1}-\Delta_n)^3+(\Delta_{n-1}-\Delta_n)^3]+\frac{3k_4A^2}{2m}(\Delta_{n+1}-\Delta_n)[\xi_{n+1}^2-2\xi_{n+1}\xi_n\cos(\phi_{n+1}-\phi_n)+\xi_n^2]\\&+\frac{3k_4A^2}{2m}(\Delta_{n-1}-\Delta_n)[\xi_{n-1}^2-2\xi_{n-1}\xi_n\cos(\phi_{n-1}-\phi_n)+\xi_n^2]\ .\end{aligned} \tag{4}$$

Analogously, a second equation is obtained by multiplying by $\cos(\omega t+\phi_n)$ before time averaging, with the result

$$\begin{aligned}\ddot{\xi}_n=&(\omega+\dot{\phi}_n)^2\xi_n+\frac{k_2}{m}[\xi_{n+1}\cos(\phi_{n+1}-\phi_n)-2\xi_n+\xi_{n-1}\cos(\phi_{n-1}-\phi_n)]\\&+\frac{2k_3A}{m}(\Delta_{n+1}-\Delta_n)[\xi_{n+1}\cos(\phi_{n+1}-\phi_n)-\xi_n]-\frac{2k_3A}{m}(\Delta_{n-1}-\Delta_n)[\xi_{n-1}\cos(\phi_{n-1}-\phi_n)-\xi_n]\\&+\frac{3k_4A^2}{m}(\Delta_{n+1}-\Delta_n)^2[\xi_{n+1}\cos(\phi_{n+1}-\phi_n)-\xi_n]+\frac{3k_4A^2}{m}(\Delta_{n-1}-\Delta_n)^2[\xi_{n-1}\cos(\phi_{n-1}-\phi_n)-\xi_n]\\&+\frac{3k_4A^2}{4m}[\xi_{n+1}\cos(\phi_{n+1}-\phi_n)-\xi_n][\xi_{n+1}^2-2\xi_{n+1}\xi_n\cos(\phi_{n+1}-\phi_n)+\xi_n^2]\\&+\frac{3k_4A^2}{4m}[\xi_{n-1}\cos(\phi_{n-1}-\phi_n)-\xi_n][\xi_{n-1}^2-2\xi_{n-1}\xi_n\cos(\phi_{n-1}-\phi_n)+\xi_n^2]\ .\end{aligned} \tag{5}$$

Finally, a third equation is obtained by time averaging over a mode period after multiplying by $\sin(\omega t+\phi_n)$:

$$\begin{aligned}\xi_n\ddot{\phi}_n=&-2\dot{\xi}_n(\omega+\dot{\phi}_n)+\frac{k_2}{m}[\xi_{n+1}\sin(\phi_{n+1}-\phi_n)+\xi_{n-1}\sin(\phi_{n-1}-\phi_n)]\\&+\frac{2k_3A}{m}[\xi_{n+1}\sin(\phi_{n+1}-\phi_n)(\Delta_{n+1}-\Delta_n)-\xi_{n-1}\sin(\phi_{n-1}-\phi_n)(\Delta_{n-1}-\Delta_n)]\\&+\frac{3k_4A^2}{m}[\xi_{n+1}\sin(\phi_{n+1}-\phi_n)(\Delta_{n+1}-\Delta_n)^2+\xi_{n-1}\sin(\phi_{n-1}-\phi_n)(\Delta_{n-1}-\Delta_n)^2]\\&+\frac{3k_4A^2}{4m}\xi_{n+1}\sin(\phi_{n+1}-\phi_n)[\xi_{n+1}^2-2\xi_{n+1}\xi_n\cos(\phi_{n+1}-\phi_n)+\xi_n^2]\\&+\frac{3k_4A^2}{4m}\xi_{n-1}\sin(\phi_{n-1}-\phi_n)[\xi_{n-1}^2-2\xi_{n-1}\xi_n\cos(\phi_{n-1}-\phi_n)+\xi_n^2]\,.\end{aligned}\tag{6}$$

Since we are assuming that the $\{\xi_n\}$, $\{\Delta_n\}$, and $\{\phi_n\}$ vary slowly with respect to the mode period, these quantities are unafffected by the time average.

Equations (4)–(6) are exactly the same as would have been obtained if instead of performing the time averages we had made a RWA-like approximation. In this approach, one first uses trigonometric identities to rewrite terms such as $\cos(\omega t+\phi_{n+1})$, occurring in the equations of motion, in terms of $\cos(\phi_{n+1}-\phi_n)\cos(\omega t+\phi_n)$ and $\sin(\phi_{n+1}-\phi_n)\sin(\omega t+\phi_n)$, and then simplifies all of the terms involving powers of $\cos(\omega t+\phi_n)$ and $\sin(\omega t+\phi_n)$ by rewriting them in terms of static quantities plus terms involving $\sin(l\omega t+\phi_n)$ and $\cos(l\omega t+\phi_n)$, where $l=1,2,3$. Equations (4)–(6) are then obtained by separately equating the static, $\sin(\omega t+\phi_n)$ and $\cos(\omega t+\phi_n)$ terms, neglecting higher-order harmonics. We note, however, that the RWA method for obtaining these equations obscures the fact that they are not applicable for rapidly growing instabilities, i.e., those whose growth rates have real or imaginary parts comparable with the mode frequency. Indeed, when such instabilities are found in our MD simulations, they are not well described by the time-average instability analysis, necessitating the more general Floquet analysis to be described in Sec. IV. Nevertheless, we will see that for the important case of slowly growing instabilities, the time-average method works very well. For simplicity, we will often refer to this method as the RWA stability analysis, although its derivation via time averaging more accurately reflects its correct physical context.

We now write $\xi_n=\xi_n^0+\delta\xi_n(t)$, $\phi_n=\delta\phi_n(t)$, and $\Delta_n=\Delta_n^0+\delta\Delta_n(t)$, where the $\{\xi_n^0\}$ and $\{\Delta_n^0\}$ are normalized dynamic and static displacements that describe the unperturbed stationary mode and where the time-dependent terms are infinitesimal perturbations. There are no $\{\phi_n^0\}$ here, since they are site independent for both the unperturbed ZBM and ILM's—these modes have adjacent particles moving π out of phase, and this is included in the $\{\xi_n^0\}$. The zeroth-order versions of Eqs. (4)–(6) are the same as the equations derived by Bickham, Kiselev, and Sievers[24] for stationary ILM's in the same (k_2,k_3,k_4) lattices considered here, namely,

$$\begin{aligned}0=&\Delta_{n+1}^0+\Delta_{n-1}^0-2\Delta_n^0+\Lambda_3[(\Delta_{n+1}^0-\Delta_n^0)^2-(\Delta_{n-1}^0-\Delta_n^0)^2]\\&+\tfrac{1}{2}\Lambda_3[(\xi_{n+1}^0-\xi_n^0)^2-(\xi_{n-1}^0-\xi_n^0)^2]+\Lambda_4[(\Delta_{n+1}^0-\Delta_n^0)^3+(\Delta_{n-1}^0-\Delta_n^0)^3]\\&+\tfrac{3}{2}\Lambda_4[(\Delta_{n+1}^0-\Delta_n^0)(\xi_{n+1}^0-\xi_n^0)^2+(\Delta_{n-1}^0-\Delta_n^0)(\xi_{n-1}^0-\xi_n^0)^2]\,,\end{aligned}\tag{7}$$

$$\begin{aligned}-\frac{\omega^2}{\omega_m^2}\xi_n^0=&\tfrac{1}{4}(\xi_{n+1}^0+\xi_{n-1}^0-2\xi_n^0)+\tfrac{1}{2}\Lambda_3[(\Delta_{n+1}^0-\Delta_n^0)(\xi_{n+1}^0-\xi_n^0)-(\Delta_{n-1}^0-\Delta_n^0)(\xi_{n-1}^0-\xi_n^0)]\\&+\tfrac{3}{4}\Lambda_4[(\Delta_{n+1}^0-\Delta_n^0)^2(\xi_{n+1}^0-\xi_n^0)+(\Delta_{n-1}^0-\Delta_n^0)^2(\xi_{n-1}^0-\xi_n^0)]\\&+\tfrac{3}{16}\Lambda_4[(\xi_{n+1}^0-\xi_n^0)^3+(\xi_{n-1}^0-\xi_n^0)^3]\,.\end{aligned}\tag{8}$$

Here we have defined the additional dimensionless cubic anharmonicity parameter $\Lambda_3\equiv k_3A/k_2$. These are the equations for *stationary* ILM's. (For the case of *traveling* ILM's, the solutions must also include an unperturbed site- and time-dependent phase.[13,24,27]) For the ZBM, $\{\Delta_n^0\}=0$, and we have only a single zeroth-order equation, which is equivalent to Eq. (3).

The first-order equations involve first time derivatives, which can be eliminated by making the substitutions $\psi_n=\delta\dot{\phi}_n/\omega$, $\zeta_n=\delta\dot{\xi}_n/\omega$, and $\rho_n=\delta\dot{\Delta}_n/\omega$. We have included the ω factors here, in anticipation of casting the first-order equations into dimensionless form. These substitutions double the number of variables, but if we assume that the perturbations have an exponential time dependence $\exp(\lambda t)$, we can reduce the problem to an eigenvalue problem involving λ/ω. The mode will be unstable if a perturbation is found having a growth rate λ with a positive real part. The six first-order equations for the nth particle are then

$$\frac{\lambda}{\omega}\rho_n=\tfrac{1}{4}\eta\{\delta\Delta_{n+1}+\delta\Delta_{n-1}-2\delta\Delta_n+2\Lambda_3[(\Delta^0_{n+1}-\Delta^0_n)(\delta\Delta_{n+1}-\delta\Delta_n)-(\Delta^0_{n-1}-\Delta^0_n)(\delta\Delta_{n-1}-\delta\Delta_n)]$$
$$+\Lambda_3[(\xi^0_{n+1}-\xi^0_n)(\delta\xi_{n+1}-\delta\xi_n)-(\xi^0_{n-1}-\xi^0_n)(\delta\xi_{n-1}-\delta\xi_n)]$$
$$+3\Lambda_4[(\Delta^0_{n+1}-\Delta^0_n)^2(\delta\Delta_{n+1}-\delta\Delta_n)+(\Delta^0_{n-1}-\Delta^0_n)^2(\delta\Delta_{n-1}-\delta\Delta_n)]$$
$$+3\Lambda_4(\Delta^0_{n+1}-\Delta^0_n)(\xi^0_{n+1}-\xi^0_n)(\delta\xi_{n+1}-\delta\xi_n)+3\Lambda_4(\Delta^0_{n-1}-\Delta^0_n)(\xi^0_{n-1}-\xi^0_n)(\delta\xi_{n-1}-\delta\xi_n)$$
$$+\tfrac{3}{2}\Lambda_4[(\xi^0_{n+1}-\xi^0_n)^2(\delta\Delta_{n+1}-\delta\Delta_n)+(\xi^0_{n-1}-\xi^0_n)^2(\delta\Delta_{n-1}-\delta\Delta_n)]\}\ , \tag{9}$$

$$\frac{\lambda}{\omega}\zeta_n=\delta\xi_n+2\xi^0_n\psi_n+\tfrac{1}{4}\eta\{\delta\xi_{n+1}+\delta\xi_{n-1}-2\delta\xi_n+2\Lambda_3[(\Delta^0_{n+1}-\Delta^0_n)(\delta\xi_{n+1}-\delta\xi_n)-(\Delta^0_{n-1}-\Delta^0_n)(\delta\xi_{n-1}-\delta\xi_n)]$$
$$+2\Lambda_3[(\xi^0_{n+1}-\xi^0_n)(\delta\Delta_{n+1}-\delta\Delta_n)-(\xi^0_{n-1}-\xi^0_n)(\delta\Delta_{n-1}-\delta\Delta_n)]$$
$$+3\Lambda_4[(\Delta^0_{n+1}-\Delta^0_n)^2(\delta\xi_{n+1}-\delta\xi_n)+(\Delta^0_{n-1}-\Delta^0_n)^2(\delta\xi_{n-1}-\delta\xi_n)]$$
$$+6\Lambda_4(\xi^0_{n+1}-\xi^0_n)(\Delta^0_{n+1}-\Delta^0_n)(\delta\Delta_{n+1}-\delta\Delta_n)+6\Lambda_4(\xi^0_{n-1}-\xi^0_n)(\Delta^0_{n-1}-\Delta^0_n)(\delta\Delta_{n-1}-\delta\Delta_n)$$
$$+\tfrac{9}{4}\Lambda_4[(\xi^0_{n+1}-\xi^0_n)^2(\delta\xi_{n+1}-\delta\xi_n)+(\xi^0_{n-1}-\xi^0_n)^2(\delta\xi_{n-1}-\delta\xi_n)]\}\ , \tag{10}$$

$$\frac{\lambda}{\omega}\psi_n=-\frac{2\zeta_n}{\xi^0_n}+\frac{\eta}{4\xi^0_n}\{\xi^0_{n+1}(\delta\phi_{n+1}-\delta\phi_n)+\xi^0_{n-1}(\delta\phi_{n-1}-\delta\phi_n)$$
$$+2\Lambda_3[\xi^0_{n+1}(\Delta^0_{n+1}-\Delta^0_n)(\delta\phi_{n+1}-\delta\phi_n)-\xi^0_{n-1}(\Delta^0_{n-1}-\Delta^0_n)(\delta\phi_{n-1}-\delta\phi_n)]$$
$$+3\Lambda_4[\xi^0_{n+1}(\Delta^0_{n+1}-\Delta^0_n)^2(\delta\phi_{n+1}-\delta\phi_n)+\xi^0_{n-1}(\Delta^0_{n-1}-\Delta^0_n)^2(\delta\phi_{n-1}-\delta\phi_n)]$$
$$+\tfrac{3}{4}\Lambda_4[\xi^0_{n+1}(\xi^0_{n+1}-\xi^0_n)^2(\delta\phi_{n+1}-\delta\phi_n)+\xi^0_{n-1}(\xi^0_{n-1}-\xi^0_n)^2(\delta\phi_{n-1}-\delta\phi_n)]\}\ , \tag{11}$$

$$\frac{\lambda}{\omega}\delta\Delta_n=\rho_n\ , \tag{12}$$

$$\frac{\lambda}{\omega}\delta\xi_n=\zeta_n\ , \tag{13}$$

$$\frac{\lambda}{\omega}\delta\phi_n=\psi_n\ , \tag{14}$$

where we have introduced the dimensionless parameter $\eta\equiv\omega_m^2/\omega^2$ in addition to Λ_3 and Λ_4. To determine λ, we need to solve a $6m\times 6m$ eigenvalue problem, where m is the number of sites included in the perturbation.

The number of sites needed to determine the stability of an ILM is restricted by the mode's localization. No analogous simplification is possible for the ZBM; however, we can use the homogeneity of the ZBM to reduce its stability analysis to an effective one-particle problem by rewriting the quantities $\{\delta\psi_n\}$, $\{\delta\Delta_n\}$, and $\{\delta\phi_n\}$ as spatial Fourier series:

$$\delta\xi_n=\sum_{kp}(-1)^n\delta\xi(k_pa)\exp(ink_pa)\ ,$$
$$\delta\phi_n=\sum_{kp}\delta\phi(k_pa)\exp(ink_pa)\ ,$$
$$\delta\Delta_n=-i\sum_{kp}\delta\Delta(k_pa)\exp(ink_pa)\ ,$$
$$\psi(k_pa)=\delta\dot{\phi}(k_pa)/\omega\ ,$$
$$\zeta(k_pa)=\delta\dot{\xi}(k_pa)/\omega\ ,$$

and

$$\rho(k_pa)=\delta\dot{\Delta}(k_pa)/\omega\ .$$

The stability equations then reduce to

$$\frac{\lambda(k_pa)}{\omega}\rho(k_pa)=-(2-\eta)\sin^2(k_pa/2)\delta\Delta(k_pa)$$
$$-\eta\Lambda_3\sin(k_pa)\delta\xi(k_pa)\ , \tag{15}$$

$$\frac{\lambda(k_pa)}{\omega}\zeta(k_pa)=\delta\xi(k_pa)+2\psi(k_pa)$$
$$-(3-2\eta)\cos^2(k_pa/2)\delta\xi(k_pa)$$
$$-2\eta\Lambda_3\sin(k_pa)\delta\Delta(k_pa)\ , \tag{16}$$

$$\frac{\lambda(k_pa)}{\omega}\psi(k_pa)=-2\zeta(k_pa)+\sin^2(k_pa/2)\delta\phi(k_pa)\ , \tag{17}$$

$$\frac{\lambda(k_pa)}{\omega}\delta\Delta(k_pa)=\rho(k_pa)\ , \tag{18}$$

$$\frac{\lambda(k_pa)}{\omega}\delta\xi(k_pa)=\zeta(k_pa)\ , \tag{19}$$

$$\frac{\lambda(k_pa)}{\omega}\delta\phi(k_pa)=\psi(k_pa)\ . \tag{20}$$

We have chosen our definitions of the Fourier coefficients so that Eqs. (15)–(20) remain simple. Note that k_pa refers to the perturbation of the ZBM envelope $\xi^0_n=(-1)^n$. Also, it is easy to see that $\lambda(k_pa)=\lambda(-k_pa)$, $\delta\Delta(k_pa)=-\delta\Delta(-k_pa)$, $\delta\psi(k_pa)=\delta\psi(-k_pa)$, and $\delta\phi(k_pa)=\delta\phi(-k_pa)$. Hence we can restrict our attention to k_pa in the range 0 to π.

B. Harmonic plus quartic case (k_2,k_4)

To more clearly elucidate the physics of the ZBM instability, we will first discuss the simpler case of a ZBM

in a harmonic plus quartic lattice. In Ref. 15, the stability of this system's ZBM was investigated using an envelope soliton approximation, which restricts the analysis to small $k_p a$ perturbations. Here we use our much less restrictive time-average analysis, which places no constraints on the perturbation wave number $k_p a$. In the absence of cubic anharmonicity, there are no static displacement perturbations $\{\delta\Delta_n\}$, and the dispersion relation for the growth rate $\lambda(k_p a)$ is given by[28]

$$\frac{\lambda^4(k_p a)}{\omega^4}+\frac{2\lambda^2(k_p a)}{\omega^2}[1+(2-\eta)\cos^2(k_p a/2)] +\sin^2(k_p a/2)[1-(3-2\eta)\cos^2(k_p a/2)]=0 . \tag{21}$$

The corresponding perturbation eigenvectors are determined from Eqs. (15)–(20). The solutions for $[\lambda(k_p a)/\omega]^2$ are real for all $k_p a$, provided $\omega/\omega_m > 1/2$. Consequently, for the systems under consideration here ($\Lambda_4 > 0$), the growth rate is always purely imaginary or purely real, producing either stable oscillating perturbations or pairs of exponentially growing (unstable) and decaying (stable) perturbations, respectively. We find that there are positive $[\lambda(k_p a)/\omega]^2$ solutions and hence unstable perturbations, provided

$$0 < k_p a < 2\cos^{-1}\left[\frac{1}{3-2\omega_m^2/\omega^2}\right]^{1/2} . \tag{22}$$

For $\omega/\omega_m > 1$, this inequality is always satisfied for some range of $k_p a$ values. Since all perturbation wavelengths are allowed for an infinite lattice, the ZBM on an infinite harmonic plus quartic lattice is *always* unstable. This result was also found by Budinsky and Bountis,[29] who determined instability thresholds for ZBM's in (k_2,k_4) lattices by using a method related to the exact Floquet method used here in Sec. IV. However, in Ref. 29 instability growth rates were not given; nor were connections made between the ZBM instability and ILM's.

For a *finite* periodic lattice, only certain wave-vector perturbations are allowed, owing to the boundary conditions. If all the $k_p a$'s satisfying Eq. (22) fall below the first nonzero allowed $k_p a$, the ZBM would be stable. However, even for a lattice as small as 20 particles, this finite-chain stability criterion is not very restrictive. For example, if k_2 and k_4 are obtained from an expansion of a Lennard-Jones potential about its minimum, the ZBM is unstable for $A/R_0 \geq 0.01$, where R_0 is the particle separation at the minimum. In the next subsection, we will show that the inclusion of cubic anharmonicity imposes a much more restrictive constraint on the appearance of the instability.

We used molecular-dynamics simulations to directly confirm our perturbation theory predictions by numerically integrating the equations of motion via the fifth-order Gear predictor-corrector method.[30] For all of the MD simulations in this paper, the mass was taken to be 39.95 amu, the lattice constant a was 1 Å, and the harmonic spring constant, when included, was $k_2 = 10.0$ eV/Å^2. The time steps were chosen such that there were at least 80 steps per mode oscillation for all runs, and the ZBM instability runs were done for a 40-particle lattice with periodic boundary conditions.

Two different methods were used to determine the growth rates for the instabilities seen in the simulations. In the first, we plot $\ln(|u_n \pm u_m|)$, where u_n and u_m are displacement maxima at appropriately chosen sites. For example, for a perturbation

$$\delta u_n \approx (-1)^n \delta\xi(k_p a)\cos(n k_p a)$$

with $k_p a = 0.2\pi$, we plot $\ln(|u_0 + u_5|)$ at the $\dot{u}_n = 0$ displacement maxima versus time. The sum eliminates the unperturbed $A(-1)^n$ terms, leaving just the perturbation, so that the slope of the plot gives the growth rate. This is the same method we used to determine the growth rates for the unstable odd-parity mode in Ref. 13. Besides this "displacement difference" method, one can also directly project out the growing displacement by taking advantage of the orthogonality of the different spatial Fourier components. Thus, at the displacement maxima,

$$\delta u(k_p a) \equiv \frac{2}{N}\sum_n \cos[n(k_p a+\pi)]u_n(t) = \pm A\,\delta\xi(k_p a)\exp(\lambda t) ,$$

and the growth rate can be determined from the slope of the $\ln|\delta u(k_p a)|$ versus time plot. For both methods, the slopes are determined by a least-squares fit to the MD data. The largest discrepancies between the two methods were found for the fastest growing perturbations, which occur for the purely quartic ZBM—faster rates mean that there are less MD data available for determining the slopes, owing to the system passing out of the region of validity of the linearized stability analysis. For the purely quartic case, the growth rates measured by these two methods differ by roughly 5%, reflecting the errors in the slopes determined from the least-squares fits. For the more general (k_2,k_4) lattices discussed below, the measured growth rates for the two methods are within $\approx 1\%$. Thus these methods typically agree very well, and in the remainder of the paper, we will use just the projection method, unless otherwise noted.

Figure 2 compares the predicted [Eq. (21)] and measured instability growth rates as a function of the perturbation wave number $k_p a$ for the ZBM in a lattice with periodic boundary conditions. The anharmonicity parameter is $\Lambda_4 = 0.068$. The MD growth rates were determined from runs for a 40-particle lattice with the ZBM seeded with the predicted phase and displacement perturbations for the $k_p a$ values under consideration. Our predicted and measured growth rates are seen to be in excellent agreement. Similar agreement was found for a much weaker anharmonicity parameter $\Lambda_4 = 0.0067$. For a Lennard-Jones potential expanded about its minimum, k_4/k_2 is approximately $50/R_0^2$, where R_0 is the particle separation at the minimum. For this value of k_4/k_2, the preceding anharmonicity parameters $\Lambda_4 = 0.068$ and $\Lambda_4 = 0.0067$ correspond to amplitudes $A/R_0 = 0.037$ and $A/R_0 = 0.012$, respectively.

As noted above, we also determined the ZBM instabili-

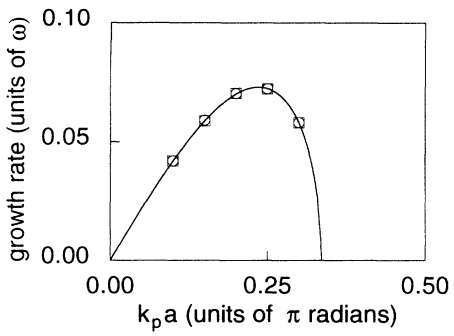

FIG. 2. Predicted and measured growth rates in units of ω, as a function of the perturbation wave number $k_p a$ for a ZBM instability perturbation in a (k_2,k_4) lattice, with periodic boundary conditions. The anharmonicity parameter is $\Lambda_4=0.068$. The solid curve gives the RWA time-average stability analysis predictions, and the symbols are obtained from MD simulations for a 40-particle lattice, using the projection method (circles) and the displacement method (squares), as discussed in the text.

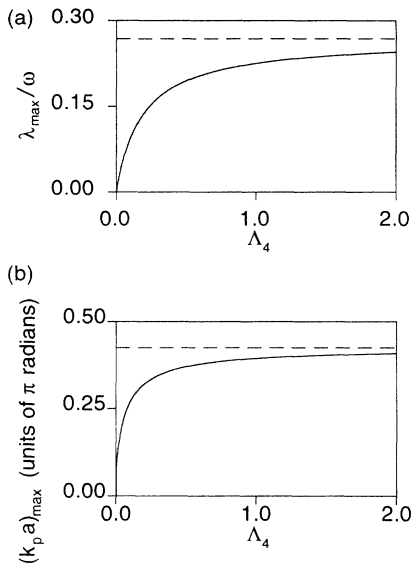

FIG. 3. RWA stability analysis predictions of (a) the largest instability growth rate λ_{max}, and (b) the corresponding wave number $(k_p a)_{max}$, as a function of the quartic anharmonicity parameter Λ_4 for ZBM's in an infinite (k_2,k_4) lattice. For reference, the dashed line gives the corresponding quantities for a purely quartic lattice. The wavelength associated with $(k_p a)_{max}$ introduces a new, anharmonicity-dependent, characteristic length scale, as discussed in the text.

ty growth rates for a purely quartic lattice. Even in this extreme case, where the fastest growing perturbation has a growth rate $\approx 25\%$ of the unperturbed ZBM frequency, the predicted and measured rates were found to differ by less than 10%. For more realistic cases, as exemplified by the $\Lambda_4=0.068$ case of Fig. 2, the predicted and measured growth rates differ by $\approx 1\%$ or less. Thus the ZBM instability in a (k_2,k_4) lattice is well described by our RWA (time-average) stability analysis.

As the anharmonicity parameter Λ_4 and hence as the ZBM frequency increases, Eq. (22) predicts that the range of $k_p a$ for which instability perturbations exist expands to include shorter-wavelength perturbations. Not only does the range of $k_p a$ for which there are instabilities increase, but the value of $k_p a$ for the fastest growing instability also increases. Figure 3 plots $k_p a$ for the fastest growing ZBM instability as a function of the anharmonicity parameter Λ_4. The wavelength associated with $(k_p a)_{max}$ introduces a new characteristic length into the problem. Figure 4 reveals that a very close relationship exists between this characteristic length and the spatial extent of the intrinsic localized modes. In this figure we compare this characteristic length with the predicted infinite lattice odd-parity ILM localization for the same frequency ZBM and odd-parity ILM's. It is appropriate to compare *equal*-frequency ILM's and ZBM's since the ZBM instabilities do not change the ZBM frequency. The odd-parity ILM localization was determined by multiplying the number of sites with displacement ξ_n^0 greater than 0.1 of the central particle displacement $\xi_0^0 \equiv 1$ by the interparticle equilibrium separation a. A similar plot is obtained when we use the even-parity ILM instead of the odd. The remarkable agreement between the ILM localization and the $(k_p a)_{max}$ wavelength strongly suggests that the characteristic length introduced by the ZBM instability is just the ILM localization.

To further investigate this connection, we must go beyond the infinitesimal perturbation regime of our stability analysis, and for this we turn to MD simulations. We find from the simulations that the instabilities follow the exponential growth predicted by the infinitesimal analysis until they reach magnitudes of roughly 10% of the unperturbed mode amplitude. Beyond this, the higher-order terms in the perturbation become important. Figures 5 and 6 give MD results showing the nonlinear evolution beyond the linear theory exponential growth regime, for the predicted fastest growing ZBM instability in a 40-particle periodic lattice. The figures are for two different values of the anharmonicity parameter Λ_4, and in each case the instability is seen to evolve into

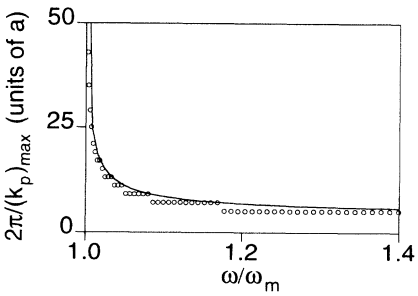

FIG. 4. Characteristic ZBM instability length scale $2\pi/(k_p)_{max}$ (solid line) and the odd-parity ILM localization (circles) as functions of the ZBM frequency and the ILM frequency, respectively, for an infinite (k_2,k_4) lattice. The ILM localization is determined by multiplying the number of sites having displacements $|\xi_n^0| \geq 0.1$ by the interparticle equilibrium separation a. The close agreement between these two quantities strongly suggests that the ILM localization is the characteristic length scale associated with the ZBM instability.

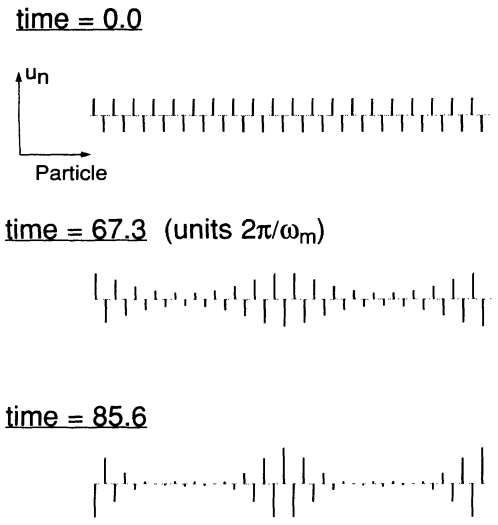

FIG. 5. *Finite* time evolution seen in a MD simulation of the predicted fastest growing ZBM instability perturbation in a 40-particle (k_2,k_4) lattice, with periodic boundary conditions. The anharmonicity parameter is $\Lambda_4=0.0067$, and the unperturbed ZBM amplitude is $A=0.015a$. The ZBM was seeded with the velocity and position perturbations predicted by our RWA stability analysis for the fastest growing ZBM instability perturbation, which occurs for $(k_pa)_{max}=0.10\pi$. The maximum amplitude for the perturbation seed is 1% of the unperturbed ZBM amplitude. The figure gives *longitudinal* displacements at the oscillation maximum; they are plotted in the vertical direction for clarity. The same vertical unit is used in each panel.

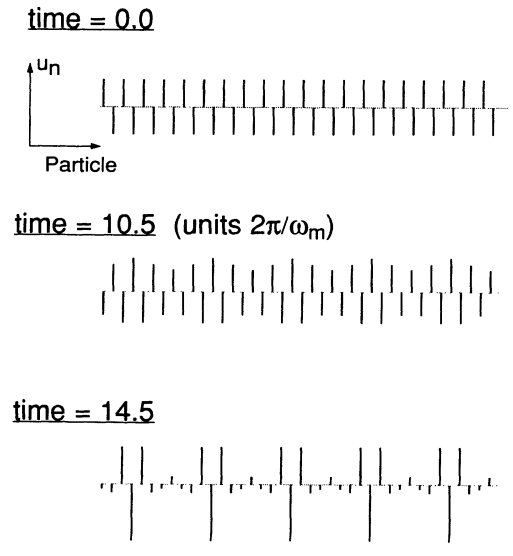

FIG. 6. Same as Fig. 5, except that here $\Lambda_4=0.068$, the unperturbed ZBM amplitude is $A=0.048a$, the fastest growing ZBM instability perturbation occurs for $k_pa=0.25\pi$, and the maximum amplitude of the perturbation seed is 0.1% of the unperturbed ZBM amplitude. Comparison with Fig. 5 shows clearly that larger anharmonicity increases the resulting finite-time vibrational localization, consistent with the connection established in Fig. 4 between the ZBM instability characteristic length scale and the ILM localization.

an array of localized excitations. Furthermore, the higher-anharmonicity ZBM evolves into more localized excitations, and consistent with the linearized theory comparisons made in Fig. 4, we find that the frequencies of the localized excitations differ by less than 1% from the corresponding unperturbed ZBM frequencies. It should be noted that the localized excitations shown in Figs. 5 and 6 are not *exact* ILM's in the sense of satisfying the equations for stationary ILM's in an infinite lattice. However, by the virtue of their localization, they strongly support our identification of the ZBM perturbation $(k_pa)_{max}$ length scale with the ILM localization, as revealed by Fig. 4.

We have thus established a close connection between the ZBM instability and ILM's in a (k_2,k_4) lattice. We have seen that the ZBM is always unstable in an infinite (k_2,k_4) lattice, and from previous work we know that ILM's always exist in such a lattice. In contrast, we will now demonstrate that the addition of *cubic* nearest-neighbor anharmonicity can stabilize the ZBM. In Sec. III we will then show that there is a direct relationship between the ZBM stability and the existence of ILM's in these more realistic lattices.

C. Harmonic, cubic, plus quartic case (k_2,k_3,k_4)

For realistic potentials, such as Lennard-Jones, the magnitude $|\Lambda_3|$ of the cubic anharmonicity parameter exceeds that of the quartic parameter Λ_4 for ZBM amplitudes below $\approx 20\%$ of the nearest-neighbor separation. Obviously then, one should include cubic as well as quartic anharmonicity when approximating these potentials. The effects of adding nearest-neighbor cubic anharmonicity upon the (k_2,k_4) ZBM instability are illustrated by Fig. 7, which compares the measured MD and predicted growth rates for ZBM's in lattices with the same quartic anharmonicity $(\Lambda_4=0.068)$, but different values of the cubic anharmonicity $(\Lambda_3=0.0,-0.096,-0.19)$. For all

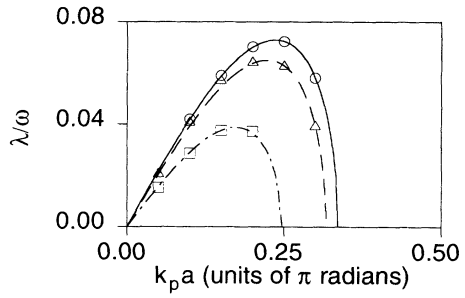

FIG. 7. Predicted and measured ZBM instability growth rates vs the perturbation wave number k_pa for a (k_2,k_3,k_4) lattice, with periodic boundary conditions. The quartic parameter Λ_4 is 0.068 for all three cases shown, and the cubic parameter Λ_3 is equal to 0.0 (solid curve), -0.096 (dashed curve), and -0.19 (dot-dashed curve). The curves give the time-average RWA method predictions, and the symbols are the corresponding growth rates measured from MD simulations for a 40-particle lattice, using the projection method. Note that as $|\Lambda_3|$ increases, the growth rates decrease. This leads to the stabilization of the ZBM against this type of instability for a sufficiently large cubic anharmonicity.

three cases, the agreement between the measured and predicted growth rates is excellent, verifying our time-averaged RWA method predictions. Furthermore, the $k_3 \neq 0$ growth rate curves are very similar to the (k_2,k_4) ZBM growth rate curves discussed in the previous section. For both the $k_3=0$ and $k_3 \neq 0$ cases shown in Fig. 7, the growth rate is zero for $k_p a=0$, increases toward a maximum as $k_p a$ increases, and then falls back to zero at a value of $k_p a$ above $(k_p a)_{\max}$. Note that the locations of both $(k_p a)_{\max}$ and the upper $\lambda(k_p a)=0$ boundary for the curves of Fig. 7 decrease as $|\Lambda_3|$ increases. This suggests that this ZBM instability might be eliminated by a sufficiently strong cubic anharmonicity.

Using these observations of the $k_3 \neq 0$ growth rate curves as a guide, a stability criterion for this ZBM instability can be determined by considering the $\lambda(k_p a)=0$ solutions of Eqs. (15)–(20). There are two such solutions. One of these is $k_p a=0$, which corresponds to the obviously stable and uninteresting ZBM perturbations consisting of an increased overall amplitude A, the addition of a constant phase to each of the particles, or a uniform translation. A second solution is determined by the equation

$$\cos(k_p a/2)=\left[3-2\eta-\frac{8\eta^2\Lambda_3^2}{2-\eta}\right]^{-1/2}, \tag{23}$$

where we recall that $\eta \equiv \omega_m^2/\omega^2=(1+3\Lambda_4)^{-1}$. For the growth rate curves shown in Fig. 7, Eq. (23) determines the upper $\lambda(k_p a)=0$ boundary for which there are unstable perturbations. Hence we expect that ZBM's with anharmonicities for which there are no real solutions to Eq. (23) most likely do not have instabilities of the form found earlier for the (k_2,k_4) ZBM's. Indeed, the exact stability analysis to be presented in Sec. IV reveals that there are at least *two* types of ZBM instabilities in (k_2,k_3,k_4) lattices. The first is similar to that found for the (k_2,k_4) ZBM's and has purely real growth rates. The second type of ZBM instability has complex growth rates which produce oscillations at frequencies comparable to the unperturbed mode frequency. Because of these rapid oscillations, this second type of instability is *not* described by our time-average analysis, which assumes a slowly varying growth rate. Nevertheless, we can still determine a stability criterion for the first type ("ILM-related") ZBM instability. For finite (k_2,k_3,k_4) lattices with periodic boundary conditions, this is done by using the smallest nonzero value of $k_p a$ allowed by the boundary conditions in Eq. (23) and rewriting the resulting equation in terms of Λ_3 and Λ_4. Applying the same procedure for an *infinite* lattice yields the ILM-related ZBM instability criterion.

$$3\Lambda_4+18\Lambda_4^2 \geq 4\Lambda_3^2 . \tag{24}$$

Here the infinite lattice solution $(k_p a=0)$ of Eq. (23) gives the equality, and the fact that the (k_2,k_4) ZBM's are unstable determines the sense of the inequality. In Sec. IV we will verify this criterion using our exact stability analysis.

III. ILM's IN (k_2,k_3,k_4) LATTICES

With cubic anharmonicity included, the ILM's are accompanied by amplitude-dependent static distortions $\{\Delta_n^0\}$ not present for $k_3=0$. Figure 8 displays the RWA-predicted frequencies as a function of mode amplitude for these more general ILM's in four 40-particle lattices having the same quartic anharmonicity $k_4/k_2=50/a^2$, but with different cubic anharmonicities $k_3/k_2=0,-8/a,-10/a,-14/a$, where we are using the equilibrium separation a as a natural unit of distance. The even- and odd-parity ILM curves are displayed in Figs. 8(a) and 8(b), respectively, and for comparison the predicted frequencies of the ZBM are also included. As discussed in Sec. II A, the ZBM frequencies with and without k_3 are identical, owing to symmetry considerations; hence there is only one ZBM curve in each panel of Fig. 8. The predicted frequencies were generated using a standard nonlinear equation solver which seeks simultaneous solutions of the equations of motion (7) and (8) for all 40 particles in these lattices. First, we obtained solutions for the largest amplitude modes using the pure quartic displacement patterns as the initial input to the

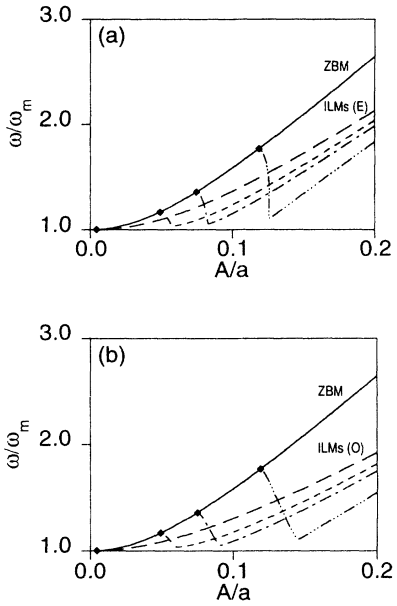

FIG. 8. Frequency vs amplitude plots predicted by the RWA for (a) the even-parity and (b) the odd-parity ILM's in four different $N=40$ periodic boundary condition lattices all with the same quartic anharmonicity $k_4/k_2=50/a^2$, but with various values for the cubic anharmonicity $(k_3/k_2=0.0,-8/a,-10/a,-14/a)$. The broken curves give the ILM frequencies, with the $|k_3|$ values at $A/a=0.2$ decreasing from bottom to top in each panel. For comparison, the solid curve in each panel gives the predicted ZBM frequencies, which are independent of k_3, and the squares give the amplitudes above which the ZBM is predicted to become unstable for the different values of the cubic anharmonicity k_3/k_2. For each value of k_3/k_2, the even- and odd-parity ILM frequencies merge with the ZBM frequency at the same amplitude, and this amplitude is also the threshold amplitude for the ZBM instability, as discussed in the text.

routine, and then we decreased the amplitude in small steps, using the solution found for the previous step as the input for the current step. We were thus able to predict frequencies, dynamic displacements, and static displacements for ILM's over a wide range of amplitudes.

For sufficiently strong cubic anharmonicity, a (k_2,k_3,k_4) interparticle potential can possess a double minimum. However, for the realistic potential functions considered in this paper, double minima are not found for (k_2,k_3,k_4) expansions about reasonable equilibrium separations.[31] Accordingly, we will restrict our attention to ILM's in single-miminum (k_2,k_3,k_4) lattices. For a $k_4/k_2=50/a^2$ lattice, the condition for a single minimum is $0\leq|k_3/k_2|\leq 14.1/a$, and it is seen that the cubic anharmonicities for the ILM's of Fig. 8 cover this range. Also, in the numerical work of this paper, we have restricted our attention to negative values of k_3, since this holds near the potential minimum of a typical interatomic potential composed of a strong repulsive part and a weaker attractive part. However, this is not a limitation, since the predictions for positive k_3 are readily obtained from the negative k_3 results given here.[32]

While the ZBM frequencies are independent of k_3, we see in Fig. 8 that the $k_3=0$ and $k_3\neq 0$ ILM frequency versus amplitude curves are quite different. For $k_3=0$, the ILM curves monotonically decrease with decreasing amplitude before merging with the ZBM curve. For the *infinite* lattice, the odd- and even-parity ILM curves would merge with the ZBM curve at zero amplitude, whereas for the $k_3=0$ 40-particle periodic boundary condition lattice results of Fig. 8, they all merge at an amplitude $A=4.6\times 10^{-3}a$ and a frequency $\omega/\omega_m=1.0016$. However, for the $k_3\neq 0$ ILM's, it is seen that just before merging with the ZBM curve, the ILM frequencies actually *increase* with decreasing amplitude over a small amplitude range, in sharp contrast to the monotonically decreasing frequencies for the $k_3=0$ case.

In order to further illustrate the difference between the $k_3=0$ and $k_3\neq 0$ ILM's, we now compare in more detail the extreme cases of Fig. 8, namely $k_3=0$ and $k_3/k_2=-14/a$. Figure 9(a) displays the frequency versus amplitude predicted by the RWA for both the odd- and even-parity ILM's and for the ZBM in the $k_3=0$ lattice, while Fig. 9(b) gives the corresponding predictions for $k_3/k_2=-14/a$. Note that for a given value of k_3, the odd- and even-parity ILM's merge with the ZBM at the same amplitude; this holds for the other two values of k_3/k_2 in Fig. 8 as well. As a check on the RWA predictions, we also include in Fig. 9 "experimental" frequencies measured in MD simulations. Our predicted and measured frequencies are found to differ by a few percent at most.

These differences between the frequency versus amplitude behavior for $k_3=0$ and $k_3\neq 0$ ILM's are reflected in their dynamical displacement patterns $\{\xi_n^0\}$. This is clearly seen in Fig. 10, where we compare the patterns for $k_3=0$ ILM's and $k_3/k_2=-14/a$ ILM's having the same frequencies. Only $k_3\neq 0$ ILM's with amplitudes greater than that for the ω/ω_m minimum in Fig. 9(b) are included in Fig. 10—the $k_3\neq 0$ ILM patterns for the region be-

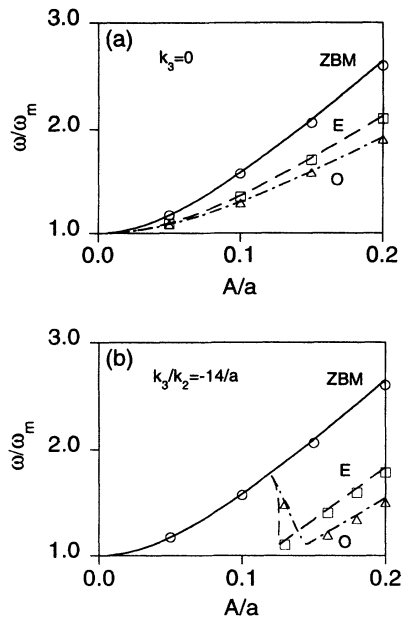

FIG. 9. Predicted frequency vs amplitude plots for the ZBM, the odd-parity ILM (O), and the even-parity ILM (E) in (a) (k_2,k_4) and (b) (k_2,k_3,k_4) $N=40$ periodic boundary condition lattices. For both lattices, $k_4/k_2=50/a^2$, and the k_3/k_2 values are labeled. The symbols are the frequencies measured from MD simulations of these modes. Note that the ILM's in the $k_3\neq 0$ case merge with the ZBM's at a significantly higher amplitude compared to the $k_3=0$ case.

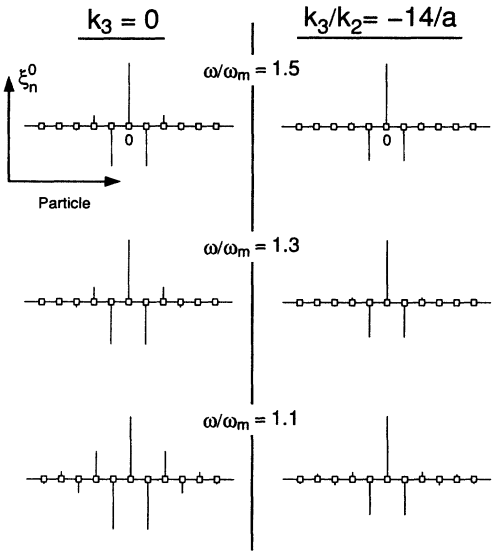

FIG. 10. Predicted odd-parity ILM dynamic displacement patterns as a function of the mode frequency for the two lattices of Fig. 9. Only patterns for modes with amplitudes to the right of the $k_3\neq 0$ odd-parity ILM frequency minimum in Fig. 9 are given here. The accompanying static distortions for the $k_3\neq 0$ cases are not shown. Note that the $k_3\neq 0$ ILM pattern remains localized as the frequency decreases, while the $k_3=0$ ILM pattern spreads out. The value of ξ_0^0 is unity for all six cases.

tween the minimum and the ZBM-ILM frequency merger will be discussed later. For the ILM's shown in Fig. 10, the $k_3 \neq 0$ modes are seen to remain highly localized on three particles as the frequency and amplitude decrease, whereas the $k_3 = 0$ mode spreads to a width of ≈ 7 particles for the lowest-frequency case.

Figure 11 displays the predicted static displacements for the lowest-frequency $k_3 \neq 0$ ILM shown in Fig. 10. The origin of the static displacements $\{\Delta_n^0\}$, which are present for $k_3 \neq 0$ but not for $k_3 = 0$ ILM's, is simply that the presence of k_3 renders the interparticle potential asymmetric, which in turn results in the particles' time-averaged displacements being amplitude dependent. Owing to the odd-parity symmetry of the mode, there is no static displacement on the central particle. However, the static displacements for all of the other particles are nonzero, and they are seen to vary strongly in the region where the dynamic displacements given by Fig. 11(a) are large. Away from the region of large dynamic displacements, the static displacements decrease linearly, so that there is a constant static strain $\{(\Delta_{n+1}^0 - \Delta_n^0)A/a\}$ away from the mode center. Indeed, for these periodic boundary condition lattices, numerical calculations show that the magnitude of this strain decreases as the total number of particles in the lattice is increased, reflecting the fact that the local "stress" introduced by the presence of the ILM is distributed over more particles.

It is interesting to note that Eq. (8) can be rewritten identically as

$$-m\omega^2 \xi_n^0 = k'_{2(n+1,n)}[\xi_{n+1}^0 - \xi_n^0] + k'_{2(n,n-1)}[\xi_{n-1}^0 - \xi_n^0] + \tfrac{3}{4}k_4 A^2[(\xi_{n+1}^0 - \xi_n^0)^3 + (\xi_{n-1}^0 - \xi_n^0)^3], \quad (25)$$

where the

$$\{k'_{2(n+1,n)} \equiv k_2 + 2k_3 A(\Delta^0{}_{n+1} - \Delta_n^0) + 3k_4 A^2(\Delta^0{}_{n+1} - \Delta_n^0)^2\}$$

are site-dependent "renormalized" harmonic force constants appropriate to the new equilibrium positions determined by the static displacements $\{\Delta_n^0\}$. The quartic anharmonicity is not renormalized, since fifth- and higher-order anharmonic terms are neglected in the (k_2, k_3, k_4) approximation. Formally, the above equation is equivalent to the RWA result for a purely quadratic plus quartic lattice which has site-dependent harmonic force constants. This site dependence is strong near the mode center, where the static displacements are rapidly varying, but away from the mode center the static strain is uniform, and the effective harmonic force constants become site independent—they are just the quasiharmonic force constants appropriate to the strained lattice. For the $k_3 \neq 0$ ILM's of Fig. 10, the dynamical behavior is thus formally similar to that of an impurity mode in a (k_2, k_4) lattice having defect-induced harmonic force constant weakening which enhances the mode's localization.

A striking feature of the $k_3 \neq 0$ ILM curves in Fig. 8 is the presence of a small amplitude range over which the ILM frequencies actually increase as the amplitude is decreased. At the lower end of this amplitude range, these ILM's have become the ZBM, and because of the symmetry of the ZBM oscillations about *each* particle equilibrium site, they have become independent of the cubic anharmonicity. As the amplitude for each of the $k_3 \neq 0$ ILM's of Fig. 8 is decreased beyond that at the minimum of ω/ω_m, their mode patterns rapidly broaden, and the role of cubic anharmonicity in their dynamics quickly decreases. Likewise, there is a rapid decrease in the size of the static displacements and the associated harmonic force constant renormalization discussed above.

As seen in Figs. 8 and 9, the odd- and even-parity ILM's for a given cubic anharmonicity merge with the ZBM at the same amplitude. This "bifurcation" amplitude is the amplitude above which ILM's exist, and it increases with increasing cubic anharmonicity for the four cases included in these figures. This amplitude is intimately connected with the threshold amplitude for ZBM instability, obtained from Eq. (23). The solid diamonds on the ZBM curves of Fig. 8 give the ZBM instability threshold amplitude for the four values of the cubic anharmonicity considered, and they are seen to be identical with the corresponding ZBM-ILM bifurcation amplitudes. This is further illustrated in Fig. 12, where the solid curve gives the 40-particle lattice ZBM instability threshold for general values of the anharmonicity parameters $\Lambda_3 \equiv k_3 A/k_2$ and $\Lambda_4 \equiv k_4 A^2/k_2$ of Sec. II, and where the circles are ZBM-ILM bifurcation points for the four values of the cubic anharmonicity of Fig. 8, together with two additional values, namely $k_3/k_2 = -6.5/a$ and $-5.0/a$. The bifurcation points for all six values of k_3/k_2 are found to fall precisely on the ZBM instability curve, with the points for larger k_3/k_2 occurring farther from the origin. Not only are the ILM-ZBM bifurcation and ZBM instability threshold

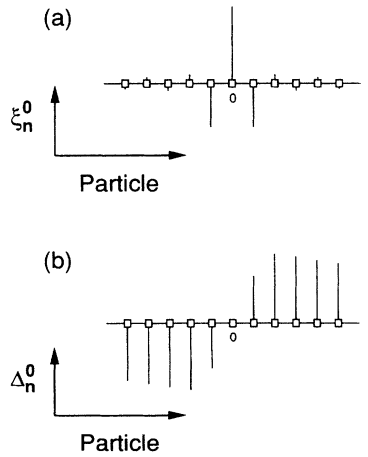

FIG. 11. Predicted (a) dynamical displacement pattern and (b) static displacements for the $\omega/\omega_m = 1.1$ $k_3 \neq 0$ odd-parity ILM shown in Fig. 10. The value of ξ_0^0 is unity, and the $\{\Delta_n^0\}$ are plotted to this scale. The static displacements locally renormalize the harmonic spring constant for this mode, as discussed in the text. There are no static displacements for the $k_3 = 0$ ILM's.

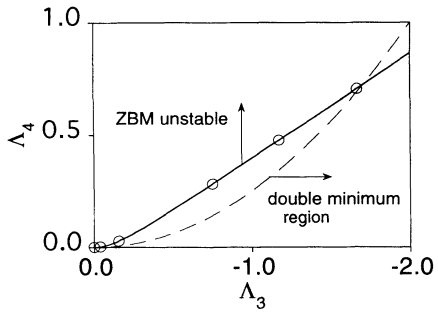

FIG. 12. Predicted RWA time-averaged method ZBM stability boundary (solid curve) as a function of the anharmonicity parameters (Λ_3,Λ_4) for a 40-particle (k_2,k_3,k_4) lattice, with periodic boundary conditions. The circles are the calculated ILM existence thresholds, which are seen to match the predicted RWA method ZBM instability thresholds. These thresholds were also found to agree for $N=6$, 10, and 20 particle periodic boundary condition lattices. We restricted our attention to single-minimum (k_2,k_3,k_4) potentials, as discussed in the text. The (Λ_3,Λ_4) values corresponding to these single-minimum potentials lie to the left of the dashed curve (Ref. 31).

amplitudes identical for these $n=40$ periodic boundary condition lattices, but the same results were found for $N=6$, 10, and 20 periodic boundary condition lattices for the same anharmonicities. *Hence, in all of these lattices, the ILM's are predicted to exist if and only if the corresponding ZBM's are unstable.*

As a further test of this conclusion, we will now compare the ILM existence threshold determined empirically for a *free* boundary condition finite lattice by Bickham, Kiselev, and Sievers[24] with our predicted RWA ZBM instability threshold for this case. Although our work has utilized *periodic* boundary conditions, it is not necessary to consider the free boundary condition case separately for this comparison; instead, we can use our infinite lattice periodic boundary condition ZBM threshold result Eq. (24), as will now be discussed. Well away from the ILM central regions, the constant static strains $\{(\Delta_{n+1}^0-\Delta_n^0)A/a\}$ occurring for $k_3\neq 0$ decrease with increasing particle numbers, as pointed out earlier, and hence vanish for the infinite lattice. In comparison, for ILM's in a one-dimensional lattice with free ends, the static strains vanish away from the mode center for both the finite and infinite lattices, provided that the dynamical displacements are well localized. Since it is just the *strains* (as opposed to the static displacements themselves) which enter the equations determining the ILM's, it is seen that within the region of nonzero dynamical displacements, the periodic boundary condition ILM's for the infinite lattice are identical with the free-end ILM's for either the infinite or finite lattice cases. (Again, this assumes that the free-end finite lattice ILM is well localized in the interior of the lattice.) Thus it is appropriate to compare our infinite lattice ZBM instability threshold Eq. (24) with the free-end ILM existence thresholds found empirically in Ref. 24. Consistent with our conclusion at the end of the previous paragraph, we find that the agreement between these thresholds is very good for (Λ_3,Λ_4) values appropriate to the single-minimum (k_2,k_3,k_4) potentials considered here. For values of $|\Lambda_3|$ outside this range, we find that the ILM existence threshold given in Ref. 24 closely follows the (k_2,k_3,k_4) double-minimum potential threshold.

We have established that for a variety of (k_2,k_3,k_4) lattices, ILM's are predicted to exist if and only if the ZBM for the same anharmonicity is unstable. Hence the ZBM instability criterion given by Eq. (24) for an infinite lattice, or by Eq. (23) for a finite lattice, is also the ILM existence criterion. This result suggests that in more general cases, such as the full realistic potentials $V(r)$ discussed in the next section, the presence of a ZBM instability in a lattice is a good indication of the existence of ILM's. However, the actual situation is more complicated than this. The exact ZBM stability analysis presented in the following section reveals that for both the case of lattices with full realistic potentials and lattices with (k_2,k_3,k_4) potentials, there exists a *second* type of ZBM instability, which is unrelated to the ILM's and is not well described by the RWA. As opposed to the RWA-predicted ILM-related ZBM instability of the present section, the new type of instability can have fast growth rates, comparable with the mode frequency. Interestingly, the new instability does not coexist with the ILM-related ZBM instability, and all of our RWA results of Secs. II and III will be unaffected.

IV. FLOQUET ZBM STABILITY ANALYSIS

A. Theory

The RWA time-averaging stability analysis of the previous sections is based upon an assumed form

$$u_n(t)=A\{[\xi_n^0+\delta\xi_n e^{\lambda t}]\cos[\omega t+\delta\phi_n e^{\lambda t}] +\Delta_n^0+\delta\Delta_n e^{\lambda t}\} \tag{26}$$

of the time-dependence, and it is further restricted to instability growth rates that are much smaller than the mode frequency. Fortunately, these approximations hold well for the instabilities discussed to this point, as is evidenced by the excellent agreement between our predicted ZBM instability growth rates and the rates measured in MD simulations. However, the RWA time-averaging method cannot ensure the stability of the ZBM against an *arbitrary* perturbation. There is always a chance that the time dependence of an instability is dramatically different from our assumed form or that an instability's growth rate violates the approximation on slowly varying quantities.

There exists a much more general method for determining the stability of nonlinear oscillations. This method is based upon Floquet's theorem,[33] and it avoids any assumptions whatsoever about the form of the perturbation and the magnitude of the growth rate. Hence, it determines the stability as well as the instability of a mode against infinitesimal perturbations. In the previous sections, we used the RWA stability analysis since it is much easier to obtain analytic results, such as the stability criterion given by Eq. (24), using this method com-

pared with the general Floquet method. Also, the RWA time-averaging method allowed us to easily separate the instability perturbations into individual contributions from the dynamical displacements, phases, and static displacements. Such a separation would have been more difficult within the Floquet method.

Before applying Floquet's theorem, we need the equations governing the time evolution of a general infinitesimal perturbation of the ZBM. To determine them, we let $r_n = u_n^0(t) + na + \delta u_n(t)$, where r_n is the position of the nth particle, a is the nearest-neighbor equilibrium separation, $u_n^0(t) = (-1)^n u^0(t)$ gives the unperturbed ZBM time-dependent displacements about the equilibrium sites, and $\delta u_n(t)$ is a time- and site-dependent infinitesimal perturbation. The linearized equations for particles interacting via nearest-neighbor potentials $V(r)$ are then

$$m\delta\ddot{u}_n = V_E[u^0(t),a](\delta u_{n+1} + \delta u_{n-1} - 2\delta u_n) - (-1)^n V_O[u^0(t),a](\delta u_{n+1} - \delta u_{n-1}) , \quad (27)$$

where

$$V_E(u^0,a) \equiv \frac{1}{2}\left[\left.\frac{d^2V(x)}{dx^2}\right|_{x=2u^0(t)+a} + \left.\frac{d^2V(x)}{dx^2}\right|_{x=-2u^0(t)+a}\right] ,$$

$$V_O(u^0,a) \equiv \frac{1}{2}\left[\left.\frac{d^2V(x)}{dx^2}\right|_{x=2u^0(t)+a} - \left.\frac{d^2V(x)}{dx^2}\right|_{x=-2u^0(t)+a}\right] .$$

The restriction to nearest-neighbor interactions will be removed shortly.

Without loss of generality, we can consider a solution of the form

$$\delta u_n(t,k_pa) = \delta u_{p1}(t,k_pa)\exp[in(k_pa+\pi)] - i\delta u_{p2}(t,k_pa)\exp[ink_pa] ;$$

a general perturbation can always be written as a linear combination of different $\delta u_n(t,k_pa)$'s. Substituting $\delta u_n(t,k_pa)$ into Eq. (27) and equating the $\exp[in(k_pa+\pi)]$ and $\exp[ink_pa]$ terms separately yields

$$\delta\ddot{u}_{p1}(t,k_pa) = -4V_E[u^0(t),a]\cos^2(k_pa/2)\delta u_{p1}(t,k_pa) - 2V_O[u^0(t),a]\sin(k_pa)\delta u_{p2}(t,k_pa) , \quad (28)$$

$$\delta\ddot{u}_{p2}(t,k_pa) = -4V_E[u^0(t),a]\sin^2(k_pa/2)\delta u_{p2}(t,k_pa) - 2V_O[u^0(t),a]\sin(k_pa)\delta u_{p1}(t,k_pa) . \quad (29)$$

These equations have the form

$$\delta\ddot{u}_{p1} = Q_{11}(t)\delta u_{p1} + Q_{12}(t)\delta u_{p2} , \quad (30)$$

$$\delta\ddot{u}_{p2} = Q_{21}(t)\delta u_{p1} + Q_{22}(t)\delta u_{p2} , \quad (31)$$

where the coefficients $Q_{ij}(t)$ are periodic functions of the ZBM period τ: $Q_{ij}(t+\tau) = Q_{ij}(t)$. In practice, for a general potential the oscillations for the unperturbed ZBM occurring in the $Q_{ij}(t)$ must be determined numerically. We accomplish this by performing molecular dynamics on the $u^0(t)$ equation of motion,

$$m\ddot{u}^0(t) = \left.\frac{dV(x)}{dx}\right|_{x=-2u^0(t)+a} - \left.\frac{dV(x)}{dx}\right|_{x=2u^0(t)+a} , \quad (32)$$

over the mode period τ. The mode period, which sets the time interval used in the MD, is determined by integrating Eq. (32) twice, which yields

$$\tau = 2\sqrt{2m}\int_0^A du\,[E - \tfrac{1}{2}V(-2u+a) - \tfrac{1}{2}V(2u+a)]^{-1/2} , \quad (33)$$

where

$$E \equiv \tfrac{1}{2}V(x)|_{x=-2A+a} + \tfrac{1}{2}V(x)|_{x=2A+a} .$$

Floquet's theorem[33] states that there are four sets of solutions to Eqs. (30) and (31) of the form

$$\delta u_{p1}(t,k_pa,j) = \exp[\lambda_j(k_pa)t]p_1(t,k_pa,j) \quad (j=1,4) , \quad (34)$$

$$\delta u_{p2}(t,k_pa,j) = \exp[\lambda_j(k_pa)t]p_2(t,k_pa,j) \quad (j=1,4) , \quad (35)$$

where $p_1(t,k_pa,j)$ and $p_2(t,k_pa,j)$ are periodic functions of time with period τ. The Appendix gives the details on how to calculate these solutions and determine the $\lambda_j(k_pa)$'s, as well as restrictions on the $\lambda_j(k_pa)$ necessary for all possible solutions to be written as linear combinations of the four solutions described above. If $\mathrm{Re}[\lambda_j(k_pa)] > 0$ for any j, we have an unstable perturbation.

If $\delta u_n(t,k_pa)$ is a solution, $\delta u_n^*(t,k_pa)$ also will be a solution. Indeed, it is easy to show from the definition of $\delta u_n(t,k_pa)$ that $\delta u_n(t,-k_pa) = \delta u_n^*(t,k_pa)$. Furthermore, the linearized equations for $\delta u_n(t,\pi-k_pa)$ reveal that

$$\delta u_n(t,\pi-k_pa) = \delta u_{p1}(t,k_pa)\exp[-ink_pa] - i\delta u_{p2}(t,k_pa)\exp[in(\pi-k_pa)] .$$

Hence we can restrict our attention to k_pa in the range $[0,\pi/2]$ and use these relations to find the solutions over the full range $[-\pi,\pi]$.

If interactions extending beyond nearest neighbors are included, Eqs. (28) and (29) become

$$\delta\ddot{u}_{p1}(t,k_pa)=-4\left\{\sum_m V_{E,2m-1}[u^0(t),a]\cos^2[(2m-1)k_pa/2]\right\}\delta u_{p1}(t,k_pa)$$
$$-4\left\{\sum_m V_{E,2m}[u^0(t),a]\sin^2(mk_pa)\right\}\delta u_{p1}(t,k_pa)$$
$$-2\left\{\sum_m V_{O,2m-1}[u^0(t),a]\sin[(2m-1)k_pa]\right\}\delta u_{p2}(t,k_pa)\ , \tag{36}$$

$$\delta\ddot{u}_{p2}(t,k_pa)=-4\left\{\sum_m V_{E,2m-1}[u^0(t),a]\sin^2[(2m-1)k_pa/2]\right\}\delta u_{p2}(t,k_pa)$$
$$-4\left\{\sum_m V_{E,2m}[u^0(t),a]\sin^2(mk_pa)\right\}\delta u_{p2}(t,k_pa)$$
$$-2\left\{\sum_m V_{O,2m-1}[u^0(t),a]\sin[(2m-1)k_pa]\right\}\delta u_{p1}(t,k_pa)\ , \tag{37}$$

where

$$V_{E,2m-1}[u^0(t),a]\equiv\frac{1}{2}\left[\left.\frac{d^2V(x)}{dx^2}\right|_{x=2u^0(t)+(2m-1)a}+\left.\frac{d^2V(x)}{dx^2}\right|_{x=-2u^0(t)+(2m-1)a}\right],$$
$$V_{E,2m}[u^0(t),a]\equiv\left.\frac{d^2V(x)}{dx^2}\right|_{x=2ma},$$
$$V_{O,2m-1}[u^0(t),a]\equiv\frac{1}{2}\left[\left.\frac{d^2V(x)}{dx^2}\right|_{x=2u^0(t)+(2m-1)a}-\left.\frac{d^2V(x)}{dx^2}\right|_{x=-2u^0(t)+(2m-1)a}\right],$$

and the sum runs over all neighbors. In practice, we limit these sums to a finite number of neighbors. Equations (36) and (37) are of the form of Eqs. (30) and (31), so that the above Floquet analysis applies.

B. (k_2,k_3,k_4) nearest-neighbor potentials

For this case, we first checked the Floquet ZBM instability predictions against our RWA time-average stability analysis results. For all of the (k_2,k_3,k_4) lattices treated in the previous sections, the RWA method predicts that the fastest growing perturbations occur for the pure k_4 case, with the maximum ZBM instability growth rate being $\lambda[(k_pa)_{\max}]=0.27\omega$. Since this is a non-negligible fraction of the unperturbed ZBM frequency ω, it should be near the limit of validity of the RWA time-average method. Hence, for the ILM-related ZBM instabilities discussed previously, the pure k_4 case is where we expect the Floquet and RWA time-averaging methods to differ the most. Figure 13 compares the instability growth rate predictions for these two methods with rates measured in MD simulations. The predicted rates for the two methods are seen not to differ by much; however, the Floquet results are clearly in better agreement with the measured rates than are the predictions of the RWA time-average method. The pure k_4 case is rather extreme—for the (k_2,k_3,k_4) values considered in the previous sections, the instability growth rates predicted by the Floquet and RWA time-averaging methods are found to be nearly identical.

Since the Floquet method is exact, it can provide stability information that the RWA cannot. In particular, it can find regions where the ZBM is *stable* against infinitesimal perturbations, as well as regions where it is unstable. Figure 14 shows the Floquet predictions for the

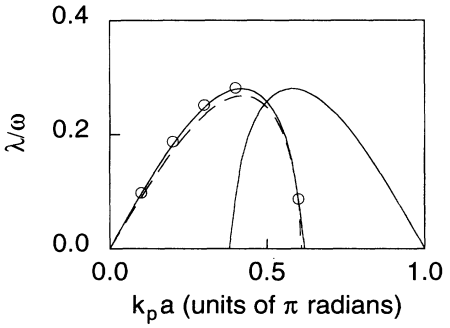

FIG. 13. Growth rates for the ZBM unstable perturbation for a purely quartic nearest-neighbor lattice with periodic boundary conditions. The solid curve gives the Floquet method prediction, the dashed curve the RWA time-average method prediction, and the circles give the growth rates measured from MD simulations for a 40-particle lattice, using the projection method. The Floquet predictions, which do not rely on the slowly varying growth rate approximation used by the RWA stability analysis, are clearly in better agreement with the MD results. The Floquet perturbations in the range $[0,\pi/2]$ are equivalent to the perturbations in the range $[\pi/2,\pi]$, as discussed in the paragraph above Eqs. (36) and (37), so that the second solid curve gives no new information.

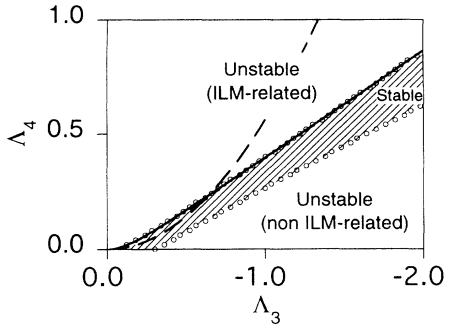

FIG. 14. Stable (shaded) and unstable (unshaded) regions predicted by the Floquet method for ZBM's in a 100-particle lattice as a function of the anharmonicity parameters Λ_3 and Λ_4. The solid curve is the instability threshold predicted by the time-averaged RWA stability analysis. Most of the unstable region in the lower right-hand portion of the figure, except for a small region in the extreme right-hand corner, corresponds to the period-doubling ZBM instability, which the RWA method fails to predict, as discussed in the text. The dashed curve gives the $[\Lambda_3(A),\Lambda_4(A)]$ values determined from the expansion of a two-particle nearest-neighbor Lennard-Jones potential about its minimum. A Floquet stability analysis for a lattice with particles interacting via the two-particle Lennard-Jones potential reveals that this (k_2,k_3,k_4) expansion breaks down before the dashed curve crosses the threshold for the ILM-related ZBM instability.

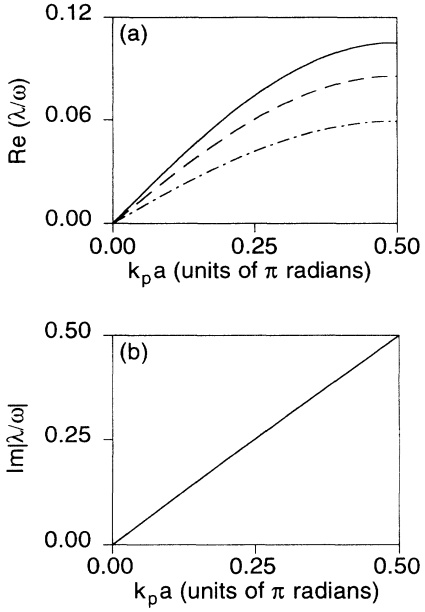

FIG. 15. Predicted (a) real and (b) imaginary parts of the growth rates as a function of the perturbation wave number $k_p a$ for unstable ZBM's in (k_2,k_3,k_4) lattices with $\Lambda_3=-0.62$ (solid curve), $\Lambda_3=-0.60$ (dashed curve), and $\Lambda_3=-0.58$ (dot-dashed curve). For all three cases, $\Lambda_4=0.10$. The Im$|\lambda(k_p a)|$ curves are the same for all three cases. These growth rate curves differ dramatically from the ILM-related ZBM instability curves shown in Figs. 2, 7, and 13.

ZBM stability and instability as a function of the cubic and quartic anharmonicity parameters Λ_3 and Λ_4. This figure was constructed by examining the stability at each (Λ_3,Λ_4) point on a 100×100 grid, with a Λ_4 range of (0,2) and a Λ_3 range of $(0,-2)$. At each (Λ_3,Λ_4) value, the stability was examined for 51 $k_p a$ points from 0 to $\pi/2$, so that we are treating a 100-particle lattice with periodic boundary conditions. These anharmonicity ranges encompass an amplitude range from zero to $|A|/a\approx0.2$ for (k_2,k_3,k_4) values evaluated at the minimum of a Lennard-Jones (LJ) potential. As will be shown later, this range extends well beyond that for which the (k_2,k_3,k_4) expansion of the LJ potential is a good approximation.

The solid curve in Fig. 14 is the RWA time-average method infinite lattice ZBM stability criterion given by Eq. (24). The instability region above this curve is thus a continuation of the ILM-related ZBM instabilities predicted by the RWA, and it duplicates the corresponding portion of Fig. 12. The circles are drawn at grid points on the boundaries between stable and unstable regions. Given the good agreement in Fig. 13 between the Floquet and RWA time-average growth rates for the ILM-related instabilities, it is not surprising that the RWA stability criterion (solid curve) falls almost exactly on the Floquet-predicted ILM-related instability boundary (upper circles) in Fig. 14. The surprise here is the existence of a new instability region, in the lower right-hand corner of the figure. Within this region, a new type of ZBM instability has been found. As opposed to the ILM-related instability, this new type of instability has complex growth rates, and Fig. 15 plots their real and imaginary parts versus $k_p a$ for three values of Λ_3 (-0.62, -0.60, and -0.58) and a fixed value of Λ_4 (0.10). These (Λ_3,Λ_4) values were chosen to lie within the single-minimum (k_2,k_3,k_4) potential region delineated in Fig. 12. A comparison between this single-minimum region and the threshold for the new ZBM instability region reveals that the two regions overlap for only a limited range of (Λ_3,Λ_4)—this is the reason for our choosing a small range of Λ_3 in Fig. 15. We will see below that this new instability also occurs in lattices with realistic potentials (e.g. Lennard-Jones), which do not possess double minima.

Before discussing Fig. 15 in detail, we give in Fig. 16 a check of our application of the Floquet method. This figure compares the $k_p a=0.4\pi$ Floquet-predicted projection

$$\frac{2}{N}\sum_n \cos[n(k_p a+\pi)]u_n(t)$$

for an unstable $\Lambda_4=0.10$ and $\Lambda_3=-0.60$ ZBM with the projection measured from a MD run of the same ZBM seeded with the predicted unstable perturbation. The Floquet predictions are in excellent agreement with the MD results until the perturbation reaches roughly 10% of the unperturbed mode amplitude. Similar agreement between predicted and observed projected perturbations are found for other values of $k_p a$ and the anharmonicity.

The preceding results dramatically validate our im-

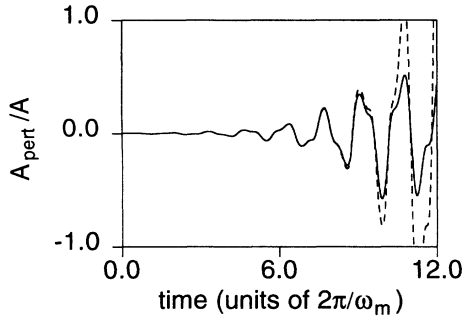

FIG. 16. Predicted and measured projected amplitudes $A_{pert}=(2/N)\sum_n \cos[n(k_pa+\pi)]u_n(t)$ for the unstable perturbations of a $(\Lambda_3,\Lambda_4)=(-0.60,0.10)$ ZBM. The solid curve is the MD result, while the dashed line is the Floquet prediction. The ZBM in the MD simulation was seeded with the $\lambda/\omega=0.081-i0.40$ $k_pa=0.4\pi$ perturbation predicted by the Floquet method calculation. Initially, the ZBM perturbation amplitude is 0.2% of the unperturbed mode amplitude. The MD and Floquet results are in excellent agreement until the projections reach about 10% of the unperturbed mode amplitude $A=0.05a$. The MD run was done for a $N=40$ particle lattice with periodic boundary conditions and potential parameters $k_4/k_2=40.0/a^2$, $k_3/k_2=-12.0/a$.

plementation of the Floquet method. However, previous studies[29,34] of the ZBM stability in (k_2,k_3) lattices $(k_4=0)$ have produced results in disagreement with those of our exact Floquet results and, moreover, contradictory to each other: In Ref. 29 the infinite lattice (k_2,k_3) ZBM was predicted to be *always* unstable, while in Ref. 34 it was predicted to be *always* stable. In contrast, as shown by the $\Lambda_4=0$ portion of Fig. 14, the exact Floquet method predicts that the (k_2,k_3) ZBM's should be stable against all infinitesimal perturbations for $|\Lambda_3|\leq 0.302$ and unstable otherwise. Furthermore, our MD simulations confirm that the $\Lambda_3=-0.303$ ZBM is indeed unstable and that the $\Lambda_3=-0.302$ ZBM remains unchanged for at least 550 oscillations. In each of these simulations, we used a 40-particle lattice with periodic boundary conditions and seeded the ZBM's with a $\delta u_{20}(t=0)=-\delta u_{21}(0)=0.0001A$ perturbation.[35] Unfortunately, the stability analysis in Ref. 34 was overly restrictive, and that of Ref. 29 appears to have been incorrectly implemented. Specifically, the method used in Ref. 34 assumed a purely sinusoidal time dependence for the unstable perturbation. We find that this is inconsistent with our Floquet results, and it is thus not surprising that the predictions of this reference disagree with our MD results. With regards to Ref. 29, the origin of the disagreement with our predictions is not obviously rooted in the stability analysis used there, since that analysis is closely related to the Floquet method. However, the conclusions drawn in this reference for the (k_2,k_3) ZBM stability are based upon a minimum energy threshold for the instability that is inconsistent with the authors' approximation $|\hat{x}^2\tan^2[(2j-1)\pi/N]|\ll 1$ (in the notation of Ref. 29), used to simplify their stability equations. A correct implementation of the method of Ref. 29 would likely require a more numerically intensive approach, similar to that used here to implement the Floquet method.

Returning to Fig. 15, we see that the growth rate versus k_pa curves for the new ZBM instability are quite different from the ILM-related instability curves examined in Secs. II and III. First, the growth rate for the new instability has a nonzero imaginary part as noted above, and for large k_pa the imaginary part violates the slowly varying approximation of the RWA time-average stability method. Second, the fastest growing instability occurs at $k_pa=0.5\pi$ for all three Λ_3 values considered in Fig. 15. Unlike the ILM-related ZBM instability, there is no evidence for a change in the preferred length scale associated with $(k_pa)_{max}$ as the anharmonicity Λ_3 changes. Since we find $\mathrm{Im}|\lambda|=0.5\omega$ for the fastest growing perturbation of this instability, we refer to it as a "period-doubling" ZBM instability. A careful examination of the predicted growth rates for (k_2,k_3,k_4) ZBM instabilities over a 10×10 grid of (Λ_3,Λ_4) values covering the range of anharmonicities displayed in Fig. 14 reveals that the new period-doubling type of instability is found over the *entire* non-ILM-related instability region shown Fig. 14, except for a small region in the lower-right hand corner, corresponding to extreme (Λ_3,Λ_4) values that are well within the double-minimum region shown in Fig. 12.

The dashed curve in Fig. 14 shows the $[\Lambda_3(A),\Lambda_4(A)]$ values obtained from a Lennard-Jones potential

$$V(r)=V_0\left[\left[\frac{R_0}{r}\right]^{12}-2.0\left[\frac{R_0}{r}\right]^{6}\right], \tag{38}$$

expanded about the potential minimum $r=R_0$. In this case $k_4/k_2=61.8/R_0^2$ and $k_3/k_2=-10.5/R_0$, independent of the strength V_0. The dashed curve shows the Lennard-Jones ZBM crossing from the stable region into the ILM-related ZBM instability region. This crossing corresponds to an amplitude of $A/R_0=0.061$. However, for this amplitude, 35% of the ZBM energy is contained in the higher-order anharmonic terms neglected in the (k_2,k_3,k_4) expansion. Hence, for these amplitudes, we must include the higher-order anharmonic terms neglected in the (k_2,k_3,k_4) expansion.

C. Full potentials

The Floquet method stability analysis can be applied for a general interparticle potential $V(r)$, with all the higher-order anharmonic terms included, as easily as it can be applied to the nearest-neighbor (k_2,k_3,k_4) potential. Furthermore, by means of Eqs. (36) and (37), the ZBM stability can also be determined for lattices with interactions extending beyond the nearest neighbors. The resulting stability boundary for the Lennard-Jones (LJ) potential of Eq. (38) is given in Fig. 17, which shows the predicted boundary between the ZBM stability and instability regions as a function of the amplitude A and equilibrium separation a. These results are independent of the potential strength V_0. The solid and dashed curves are the predicted boundaries for lattices with LJ interactions extended to six nearest neighbors and to nearest

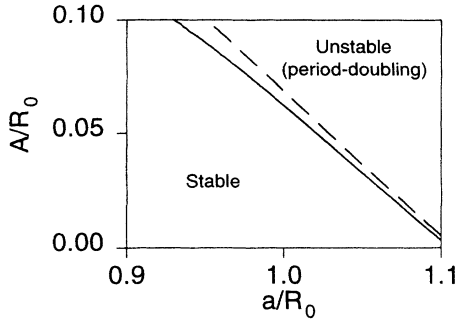

FIG. 17. Floquet-method-predicted ZBM stability boundary as a function of the mode amplitude A and equilibrium separation a for a one-dimensional lattice with particles interacting via a Lennard-Jones potential. The solid curve is the prediction for a lattice with the interactions extending to six nearest neighbors, and the dashed curve gives the prediction for a lattice with interactions restricted to nearest neighbors. Including interactions beyond the six nearest neighbors does not significantly alter the stability boundary.

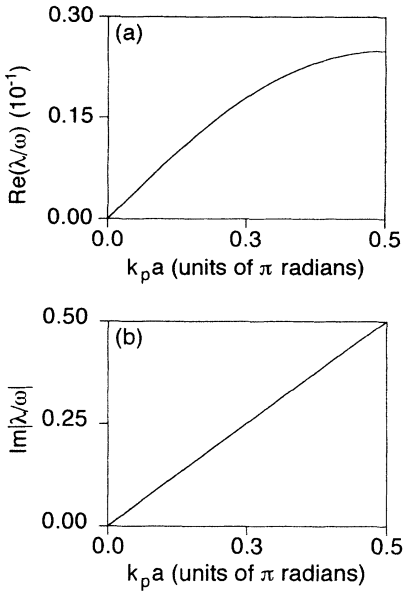

FIG. 18. Floquet-stability-method-predicted (a) real and (b) imaginary parts of the unstable ZBM growth rate as a function of the perturbation wave number $k_p a$ for a one-dimensional lattice with particles interacting via a Lennard-Jones potential and with interactions extending out to the six nearest neighbors. The unperturbed ZBM amplitude is $A=0.065R_0$, and the equilibrium separation is $a=R_0$. These growth rate curves have the same form as the curves given in Fig. 15 for the period-doubling ZBM instability predicted for the (k_2,k_3,k_4) lattices. Such growth rate vs $k_p a$ curves are predicted throughout the ZBM unstable region shown in Fig. 17, and no ILM-related instabilities are found.

neighbors, respectively. We could have included more than six nearest neighbors in the former calculation, but we found that the position of the ZBM stability boundary did not change noticeably with the addition of interactions beyond six neighbors.

The predicted real and imaginary parts of the ZBM instability growth rates versus the perturbation wave vector $k_p a$ for an amplitude $A/R_0=0.065$ and equilibrium separation $a/R_0=1.0$ ZBM are shown in Fig. 18 for a six nearest-neighbor interaction LJ lattice. These curves closely resemble those shown in Fig. 15 for the (k_2,k_3,k_4) period-doubling instability. Moreover, such growth rate versus $k_p a$ curves have been found throughout the LJ unstable ZBM regions shown in Fig. 17 for both six nearest-neighbor and nearest-neighbor interaction LJ lattices. No evidence of the ILM-related instability was found in either type of LJ lattice. Since the period-doubling ZBM instability occurs in the nearest-neighbor interaction LJ lattice, as well as in the extended interaction LJ lattices, the presence of this new instability and the absence of the ILM-related instability in the full potential must be due to the higher-order anharmonic terms in the potential, which are neglected in our earlier (k_2,k_3,k_4) model.

Turning to other forms of the potential $V(r)$, we show in Fig. 19 the predicted ZBM instability boundaries for a lattice of particles interacting via a nearest-neighbor Born-Mayer plus Coulomb (BMC) potential

$$V_{\mathrm{BMC}}(r)=\lambda e^{-r/\rho}-\frac{q^2e^2}{r} \tag{39}$$

and nearest-neighbor Morse potential

$$V_{\mathrm{Morse}}(r)=D_e[1-e^{-B_e(r-r_e)}]^2-D_e\ . \tag{40}$$

The Born-Mayer parameters are taken from a fit to breathing shell model nearest-neighbor harmonic force constants for KI at $T=0$ K ($\lambda=8.47\times10^{-8}$ ergs, $\rho=0.26$ Å, $q=0.9$),[36] while the Morse parameters are from a fit to the $^{35}Cl_2$ molecular spectrum ($B_e=4.06/r_e$).[37] For these potentials, the potential minima are $R_0=3.14$ Å (BMC) and $R_0=r_e$ (Morse). As was the case with the LJ potential, we find that growth rate versus $k_p a$ curves for the unstable ZBM's in the BMC

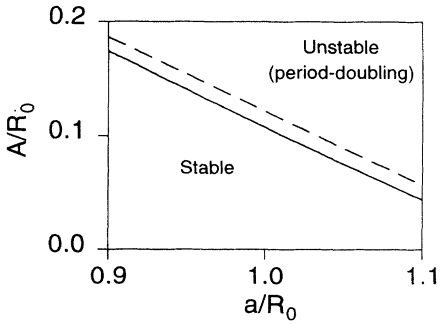

FIG. 19. Floquet-stability-method-predicted ZBM stability boundaries as a function of the mode amplitude A and equilibrium separation a for ZBM's in a one-dimensional lattice with particles interacting via a Morse (solid curve) and Born-Mayer plus Coulomb (dashed curve) potential. For both cases, the interaction is restricted to nearest neighbors. The predicted growth rate vs perturbation wave number $k_p a$ curves for ZBM's in the Morse and Born-Mayer unstable ZBM regions are of the period-doubling type shown in Fig. 18 for a ZBM in a lattice with particles interacting via a Lennard-Jones potential.

and Morse lattices are only of the period-doubling type shown in Figs. 15 and 18. Moreover, as in the LJ case, no ILM-related ZBM instabilities are found. Figure 20 compares these three potential functions, with each normalized so that the well depths and potential minimum separations are the same. Since the ZBM stability equations can be cast into a dimensionless form independent of the exact value of the potential strength and potential minimum separation, this is an appropriate comparison. The details, such as the strength of the attractive portion of the potential, are different for these three potentials; however, they all share the common characteristic that they have a strong repulsive and weaker attractive term. The period-doubling ZBM instability also occurs in (k_2,k_3,k_4) lattices for (Λ_3,Λ_4) values where the potential asymmetry introduced by k_3 is important, whereas this instability weakens as the quartic anharmonicity increases and the asymmetry becomes less important. Based upon these observations, we expect that this new ZBM instability will be a general feature of strongly asymmetric potentials.

Figures 17 and 19 show that the small-amplitude ZBM in lattices with realistic potentials is stable. For instance, the equilibrium separation for a six-particle interaction LJ lattice is $a=0.997R_0$, and the predicted amplitude criterion for ZBM instability in this case is $A/R_0 \geq 0.063$. This is a very large amplitude: Such a ZBM contains 99% of the energy necessary to dissociate the crystal. For ZBM's vibrating about the minimum energy equilibrium separation in Morse and BM potentials, this instability criterion corresponds to even higher A/R_0's, in terms of the appropriate R_0 for each potential. However, as the equilibrium separation a increases, the amplitude threshold for the period-doubling ZBM instability decreases. A typical change in the lattice constant due to thermal expansion for simple materials, such as rare gas crystals, alkali halides, and simple metals, is roughly 3% in going from absolute zero to the melting temperature.[38] A 3% increase in the equilibrium separation from $a=R_0$ to $a=1.03R_0$ decreases the LJ ZBM instability amplitude threshold for a six-particle interaction lattice by $\Delta A=0.017R_0$. At this new equilibrium separation and instability threshold amplitude, the ZBM energy has lowered to roughly 22% of the dissociation energy.

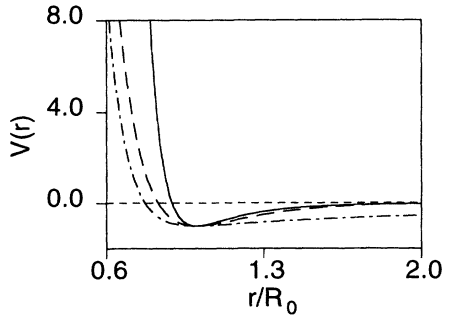

FIG. 20. Lennard-Jones (solid curve), Morse (dashed curve), and Born-Mayer plus Coulomb (dot-dashed curve) potentials used in the text. For this comparison, the strength of the potentials and the nearest-neighbor separations were adjusted so that the potential minimums for the three potentials match. All three potentials are characterized by a strong repulsion and a weaker attraction. However, the strength of these repulsive and attractive terms varies substantially among these three potentials.

In Fig. 17, we see that the inclusion of more neighbors in the ZBM stability calculation also lowers the ZBM instability threshold. In fact, in going from a lattice with only nearest-neighbor interactions to a lattice with interactions extending to the sixth nearest neighbors, most of the decrease in the ZBM instability threshold is due to the second neighbors. In higher-dimensional crystals, the second neighbors are usually closer together than in the 1D case, and the effects of longer-range interactions on the ZBM stability could be enhanced.

D. Full potentials and ILM's

By using quartic, cubic, and quadratic nearest-neighbor force constants obtained from the LJ potential in our (k_2,k_3,k_4) model, one might conclude that the ILM's can exist in a lattice of particles interacting with nearest-neighbor LJ potentials. (See the dashed curve of Fig. 14.) However, we have shown that the higher-order anharmonic terms neglected in the (k_2,k_3,k_4) model actually prevent the ILM-related ZBM instability from occurring for a LJ potential. Given the strong connection that we have established between the ILM's and ZBM instability for (k_2,k_3,k_4) lattices, we expect that ILM's will not exist if this ZBM instability does not occur. However, we have not proved this for a general potential, and we therefore need to look directly for the ILM's in lattices with realistic potentials. In order to do this for a full potential where the higher-order anharmonic terms are important, we first substitute the trial solution $r_n = A\xi_n^0 \cos(\omega t) + A\Delta_n^0 + nR_{\rm eq}$ into the equations of motion,

$$m\ddot{r}_n = -\frac{\partial V(\mathbf{r})}{\partial r_n} , \tag{41}$$

where r_n is the nth particle position and $V(\mathbf{r})$ is a general potential involving all the particles in the lattice. Then, in the spirit of the RWA, we time average the equations of motion over a mode period to obtain the full potential counterpart to Eq. (7). To obtain the full potential equation corresponding to Eq. (8), we multiply Eq. (41) by $\cos(\omega t)$ before time averaging. In practice, these time averages often need to be done numerically for a general potential. The resulting equations are then solved by a standard nonlinear equation solver. We checked this procedure using the ZBM—we compared the exact ZBM period τ for a LJ lattice with the RWA-predicted period $\tau=2\pi/\omega$ and found that they differ by less than 5% for amplitudes $A/R_0 \leq 0.14$.

Using this method, we searched for ILM solutions over an amplitude range $0.01 \leq A/R_0 \leq 0.20$ and equilibrium separation range $0.90 \leq a/R_0 \leq 1.1$, in both the nearest-neighbor interaction and sixth nearest-neighbor interaction LJ lattices. We found no ILM solutions. Because no ILM's were found directly and because of the absence of

an ILM-related ZBM instability, we conclude that ILM's do not exist in these lattices. Similar results were found for lattices interacting via the Morse and BMC potentials.

For *diatomic* one-dimensional (k_2,k_3,k_4) lattices Kiselev, Bickham, and Sievers[25] found ILM's in both the harmonic gap and for $\omega/\omega_m > 1$. (Here ω_m is the corresponding maximum diatomic lattice harmonic phonon frequency.) Furthermore, they found no evidence of the $\omega/\omega_m > 1$ ILM's for diatomic lattices when the (k_2,k_3,k_4) potentials were replaced by realistic nearest-neighbor potentials, whereas they found that the gap ILM's were retained. These results for the $\omega/\omega_m > 1$ diatomic ILM's are qualitatively very similar to the results we have found here for ILM's in monatomic lattices. However, in Ref. 25, connections were not established between the diatomic ILM's and a diatomic lattice extended anharmonic mode, analogous to the ILM-ZBM connection studied here.

V. CONCLUSIONS

For periodic one-dimensional monatomic lattices with harmonic, cubic, and quartic nearest-neighbor interactions (k_2,k_3,k_4) we have shown that the anharmonic ZBM is unstable against infinitesimal perturbations for a range of values of the cubic and quartic anharmonicity parameters $\Lambda_3=k_3A/k_2$ and $\Lambda_4=k_4A^2/k_2$. This has been done by developing both a RWA time-average method and an exact Floquet method for determining the ZBM stability, and by testing the predictions of these stability theories using molecular-dynamics simulations.

The exact Floquet analysis reveals that there are two types of ZBM instabilities in these lattices for (Λ_3,Λ_4) values corresponding to single-minimum (k_2,k_3,k_4) lattices. The first type is intimately connected with the existence of ILM's, and it is also well described by the RWA time-average instability method, whereas the second type is not well described by the RWA method and is not related to ILM's.

The ILM-related ZBM instability always exists for infinite lattices with harmonic plus quartic nearest-neighbor interactions $(k_3=0)$. It is characterized by purely real growth rates which are smaller than the ZBM frequency, and the Fourier component corresponding to the fastest-growing unstable perturbation introduces an anharmonicity-dependent length scale, which we have shown matches the ILM localization in these (k_2,k_4) lattices. Over finite times, this fastest growing unstable ZBM perturbation leads to the ZBM evolving into a periodic array of localized excitations which are qualitatively similar to the isolated ILM's. With the addition of cubic anharmonicity, the ILM-related instability is found to persist; however, it can be eliminated if the cubic anharmonicity is made sufficiently strong. For given values of k_4/k_2 and k_3/k_2, this stabilization is characterized by an amplitude threshold below which the ZBM is stable. For a wide variety of finite (k_2,k_3,k_4) lattices with periodic boundary conditions, we have shown that this ZBM instability threshold is identical with the amplitude threshold for existence of ILM's. Hence we conclude that in (k_2,k_3,k_4) lattices, ILM's with a given amplitude will exist if and only if an ILM-related instability occurs for the ZBM with the same amplitude. This result suggests that, in general, the presence of the ILM-related ZBM instability in a lattice is a good indication of the existence of intrinsic localized modes.

In a previous study of ILM stability, we found that the RWA time-average instability method accurately predicts ILM instability growth rates for the (k_2,k_4) ILM's.[13] Moreover, as just noted, the RWA method accounts very well for the ILM-related instability of the ZBM studied in this paper. It is a convenient method within its sphere of validity, often lending itself to the derivation of useful analytic results such as the ZBM instability criteria obtained here. However, the RWA method relies upon assumptions about the form and time dependence of the perturbations, and it is thus inadequate for some types of instability, such as those with rapid growth rates. In comparison, the Floquet method used here in Sec. IV is exact; it requires only that the ZBM perturbations be small enough that they can be treated as infinitesimals. The use of the exact Floquet stability analysis of the ZBM reproduced the RWA results, but it also revealed the presence of a new instability, unrelated to the ILM's and not well described by the RWA.

In contrast to the purely real growth rates and anharmonicity-dependent ILM-related length scales found for the ILM-related ZBM instability, the new instability is characterized by complex growth rates having large oscillatory components, which can be comparable in size to the unperturbed mode frequency, and by an anharmonicity-*independent* length scale. Furthermore, this "period-doubling" type of ZBM instability occurs for (k_2,k_3,k_4) ZBM's with a strong nearest-neighbor cubic anharmonicity, while the ILM-related type of instability is found for ZBM's dominated by quartic interactions. Our general Floquet stability analysis shows that the ZBM is also unstable in lattices with particles interacting via realistic Lennard-Jones, Morse, or Born-Mayer plus Coulomb potentials. However, unlike the case of (k_2,k_3,k_4) lattices, the presence of higher-order anharmonic terms in these potentials results in *no* ILM-related instabilities being found. Rather, the ZBM instabilities for these realistic potentials are of the period-doubling type. Given the strong connection which we established between the ILM's and ZBM stability in (k_2,k_3,k_4) lattices, the absence of the ILM-related ZBM instability in lattices with the full realistic potentials strongly suggests that ILM's do not exist in such lattices. Nor did we find ILM's in these lattices when we looked for them using direct numerical searches. Based upon the absence of the ILM-related ZBM instability, together with our inability to find these modes directly, we conclude that ILM's indeed do not exist in these realistic potential lattices.

Each of the three potential functions treated here is characterized by a strong repulsive interaction and a weaker attractive interaction. However, the strengths of these interactions are quite different for the individual potentials. Given that the period-doubling ZBM instability occurs for all three potentials, we expect that the period-doubling ZBM instability will be a general feature of po-

tentials having a strong repulsive interaction and a weaker attractive interaction. Furthermore, the amplitude threshold for this ZBM instability was found to decrease as the lattice expands, indicating that this instability might occur for a similar extended anharmonic phonon mode in realistic three-dimensional crystals at high temperatures.

We have already seen that one type of ZBM instability is intimately related to the presence of intrinsic local modes in homogeneous lattices with nonlinear intersite coupling. Moreover, the results of other calculations indicate that such a relationship between local and extended anharmonic modes occurs for other physical situations, such as one-dimensional lattices with on-site anharmonicity,[18] two-dimensional lattices with nonlinearly coupled rotating dipoles,[39] and small molecules.[40] However, the physical implications of the period-doubling ZBM instability found here are not yet clear. Studies of related but much simpler $N=3$ degrees of freedom Hamiltonian systems show that the onset of large-scale chaos throughout phase space can be connected with instabilities of simple periodic oscillations.[29] It remains to be seen whether or not the ZBM period-doubling instability plays such a role in the lattices considered here.

ACKNOWLEDGMENTS

The research by K.W.S. and J.B.P. was supported by NSF Grant No. DMR-9014729. J.B.P. gratefully acknowledges the support of the Alexander von Humboldt Foundation during a portion of this work. K.W.S. acknowledges partial support from the Achievement Rewards for College Scientists. We thank T. Rössler for helpful discussions.

APPENDIX: FLOQUET STABILITY METHOD

In the main text, we outlined the Floquet method used to determine the ZBM stability. Here we give additional details on why this method works and how we implemented it. This presentation closely follows the Floquet theorem proofs given in Refs. 33.

The linearized equations for the ZBM Fourier-analyzed perturbation have the form

$$\ddot{y}=Q_{11}(t)y+Q_{12}(t)u \ , \tag{A1}$$

$$\ddot{u}=Q_{12}(t)y+Q_{22}(t)u \ , \tag{A2}$$

where the coefficients are periodic in time $Q_{ij}(t+\tau)=Q_{ij}(t)$ with a period τ. Solutions to these equations are uniquely determined by specifying the initial conditions $y(0)$, $\dot{y}(0)$, $u(0)$, and $\dot{u}(0)$. Since this is a linear problem where superposition applies, we can *always* write a general solution as a linear combination of a set of four basic solutions which satisfy the initial conditions

$$\begin{aligned}
&y_1^0(0)=1, \ \dot{y}_1^0(0)=0, \ u_1^0(0)=0, \ \dot{u}_1^0(0)=0 \ , \\
&y_2^0(0)=0, \ \dot{y}_2^0(0)=1, \ u_2^0(0)=0, \ \dot{u}_2^0(0)=0 \ , \\
&y_3^0(0)=0, \ \dot{y}_3^0(0)=0, \ u_3^0(0)=1, \ \dot{u}_3^0(0)=0 \ , \\
&y_4^0(0)=0, \ \dot{y}_4^0(0)=0, \ u_4^0(0)=0, \ \dot{u}_4^0(0)=1 \ .
\end{aligned} \tag{A3}$$

Furthermore, we can express any one of these fundamental solutions evaluated at time $t+\tau$ as a sum of all four fundamental solutions evaluated at time t:

$$\begin{aligned}
y_n^0(t+\tau)=&y_n^0(\tau)y_1^0(t)+\dot{y}_n^0(\tau)y_2^0(t) \\
&+u_n^0(\tau)y_3^0(t)+\dot{u}_n^0(\tau)y_4^0(t) \ ,
\end{aligned} \tag{A4}$$

$$\begin{aligned}
u_n^0(t+\tau)=&y_n^0(\tau)u_1^0(t)+\dot{y}_n^0(\tau)u_2^0(t) \\
&+u_n^0(\tau)u_3^0(t)+\dot{u}_n^0(\tau)u_4^0(t) \ .
\end{aligned} \tag{A5}$$

Note that these expressions give the correct initial conditions at $t=0$.

We are going to seek solutions of the form $y(t+\tau)=\rho y(t)$, $u(t+\tau)=\rho u(t)$. If such solutions can be found, they can always be written in the form

$$y(t)=e^{i\alpha t}v(t) \ ,$$

$$u(t)=e^{i\alpha t}w(t) \ ,$$

where $v(t)$ and $w(t)$ are periodic functions of time with period τ and $\exp(i\alpha\tau)=\rho$. Since the $\{y_n^0(t)\}$ and $\{u_n^0(t)\}$ form a complete basis, we can also write

$$y(t)=\sum_{n=1}^{4} c_n y_n^0(t) \ ,$$

$$u(t)=\sum_{n=1}^{4} c_n u_n^0(t) \ ,$$

and the solutions we seek can then be expressed as

$$y(t+\tau)=\rho\sum_{n=1}^{4} c_n y_n^0(t)=\sum_{n=1}^{4} c_n y_n^0(t+\tau) \ , \tag{A6}$$

$$u(t+\tau)=\rho\sum_{n=1}^{4} c_n u_n^0(t)=\sum_{n=1}^{4} c_n u_n^0(t+\tau) \ . \tag{A7}$$

Equations (A4) and (A5) express the $\{y_n^0(t+\tau)\}$ and $\{u_n^0(t+\tau)\}$ in terms of the $\{y_n^0(t)\}$ and $\{u_n^0(t)\}$. Once this is done, Eqs. (A6) and (A7) reduce to two identical eigenvalue problems involving the coefficients $\{c_n\}$ and ρ,

$$\rho\mathcal{C}=\begin{bmatrix}
y_1^0(\tau) & y_2^0(\tau) & y_3^0(\tau) & y_4^0(\tau) \\
\dot{y}_1^0(\tau) & \dot{y}_2^0(\tau) & \dot{y}_3^0(\tau) & \dot{y}_4^0(\tau) \\
u_1^0(\tau) & u_2^0(\tau) & u_3^0(\tau) & u_4^0(\tau) \\
\dot{u}_1^0(\tau) & \dot{u}_2^0(\tau) & \dot{u}_3^0(\tau) & \dot{u}_4^0(\tau)
\end{bmatrix}\mathcal{C} \ , \tag{A8}$$

where $\tilde{\mathcal{C}}\equiv\{c_1,c_2,c_3,c_4\}$. This equation is of the standard eigenvalue form $(\rho\mathbf{I}-\mathbf{A})\mathcal{C}=0$, and the eigenvalue ρ will thus be determined by the condition $|\rho\mathbf{I}-\mathbf{A}|=0$. This condition gives

$$\rho=e^{\pm i\alpha_1\tau}, \ e^{\pm i\alpha_2\tau} \ , \tag{A9}$$

where the α_j are, in general, complex numbers determined by

$$\cos(\alpha_1\tau)=b_1+a_1 ,$$

$$\cos(\alpha_2\tau)=b_1-a_1 ,$$

$$b_1=\tfrac{1}{4}[y_1^0(\tau)+\dot{y}_2^0(\tau)+u_3^0(\tau)+\dot{u}_4^0(\tau)] ,$$

$$\begin{aligned} a_1=\tfrac{1}{2}\{\tfrac{1}{4}[&y_1^0(\tau)+\dot{y}_2^0(\tau)-u_3^0(\tau)-\dot{u}_4^0(\tau)]^2 \\ &+2-u_3^0(\tau)\dot{u}_4^0(\tau)+u_4^0(\tau)\dot{u}_3^0(\tau)-y_1^0(\tau)\dot{y}_2^0(\tau) \\ &+y_2^0(\tau)\dot{y}_1^0(\tau)+y_3^0(\tau)u_1^0(\tau)+y_4^0(\tau)\dot{u}_1^0(\tau) \\ &+\dot{y}_3^0(\tau)u_2^0(\tau)+\dot{y}_4^0(\tau)\dot{u}_2^0(\tau)\}^{1/2} . \end{aligned}$$

The determination of α_1 and α_2 requires knowledge of $y_j^0(\tau)$, $\dot{y}_j^0(\tau)$, $u_j^0(\tau)$, and $\dot{u}_j^0(\tau)$. We have determined these values by numerically integrating Eqs. (A1) and (A2) using the appropriate initial conditions.

Since the entries in the matrix appearing in Eq. (A8) are real, if ρ is an eigenvalue, then the complex conjugate ρ^* will also be an eigenvalue. Furthermore, the form of the solutions given in Eq. (A9) shows that if ρ is a eigenvalue, then so is $1/\rho$. Based on these observations, the four growth rates $\lambda=\pm i\alpha_1,\pm i\alpha_2$ determined by the ZBM stability analysis for each k_pa value can be sorted into the following four groups: (1) α_1 and α_2 both real, (2) α_1 and α_2 both pure imaginary, (3) $\alpha_1=\pm(\alpha+i\beta)$ and $\alpha_2=\pm(\alpha-i\beta)$, and (4) $\alpha_1=\pm\alpha$ and $\alpha_2=\pm i\beta$, where α and β are both real and nonzero. Comparing these groupings with the results presented in the text, we see that the purely real growth rates for the ILM-related instability belong to groups (2) and (4), while the complex growth rates for the period-doubling instability belong to group (3).

The set of four solutions corresponding to the different values of ρ will be linearly independent and thus form a basis for all possible solutions if all four values of ρ are distinct.[33] Otherwise, the solutions need to be examined on a case-by-case basis. We have checked our ZBM stability solutions for ρ against this criterion and found that it has been violated in only two cases. The first case is for $k_pa=0$. This turns out to be a trivial case, since the four linearly independent $k_pa=0$ solutions correspond to a uniform translation of the lattice, uniform center-of-mass motion, a constant phase shift for the ZBM, and a change in the ZBM amplitude. None of these changes produces an instability. The second case is $k_pa=0.5\pi$. In this case, $Q_{11}(t)=Q_{22}(t)$, and we can define new variables $v_+(t)=y(t)+u(t)$ and $v_-(t)=y(t)-u(t)$, which decouple Eqs. (A1) and (A2):

$$\ddot{v}_+(t)=[Q_{11}(t)+Q_{12}(t)]v_+(t) , \tag{A10}$$

$$\ddot{v}_-(t)=[Q_{11}(t)-Q_{12}(t)]v_-(t) . \tag{A11}$$

Each of these equations can be solved separately. Furthermore, they must reproduce the same solutions that we found before making this separation. We can now apply results developed for these uncoupled equations and conclude that the four solutions will be linearly independent unless $|\rho|=1$,[33] a condition which never occurred in our application of the Floquet method.

[1]A. S. Dolgov, Fiz. Tverd. Tela (Leningrad) **28**, 1641 (1986) [Sov. Phys. Solid State **28**, 907 (1986)].

[2]A. J. Sievers and S. Takeno, Phys. Rev. Lett. **61**, 970 (1988).

[3]S. Takeno, K. Kisoda, and A. J. Sievers, Prog. Theor. Phys. Suppl. **94**, 242 (1988).

[4]J. B. Page, Phys. Rev. B **41**, 7835 (1990).

[5]R. Bourbonnais and R. Maynard, Phys. Rev. Lett. **64**, 1397 (1990).

[6]V. M. Burlakov, S. A. Kiselev, and V. N. Pyrkov, Solid State Commun. **74**, 327 (1990).

[7]V. M. Burlakov, S. A. Kiselev, and V. N. Pyrkov, Phys. Rev. B **42**, 4921 (1990).

[8]S. A. Kiselev, Phys. Lett. A **148**, 95 (1990).

[9]S. Takeno, J. Phys. Soc. Jpn. **59**, 3861 (1990).

[10]R. Bourbonnais and R. Maynard, Int. J. Mod. Phys. C **1**, 233 (1990).

[11]S. R. Bickham and A. J. Sievers, Phys. Rev. B **43**, 2339 (1991).

[12]K. Yoshimura and S. Watanabe, J. Phys. Soc. Jpn. **60**, 82 (1991).

[13]K. W. Sandusky, J. B. Page, and K. E. Schmidt, Phys. Rev. B **46**, 6161 (1992).

[14]V. M. Burlakov, S. A. Kiselev, and V. I. Rupasov, Pis'ma Zh. Eksp. Teor. Fiz. **51**, 481 (1990) [JETP Lett. **51**, 544 (1990)]; Phys. Lett. A **147**, 130 (1990).

[15]V. M. Burlakov and S. A. Kiselev, Zh. Eksp. Teor. Fiz. **99**, 1526 (1991) [Sov. Phys. JETP **72**, 854 (1991)].

[16]Y. S. Kivshar, Phys. Rev. E **48**, 4132 (1993).

[17]Y. S. Kivshar and M. Peyrard, Phys. Rev. A **46**, 3198 (1992).

[18]T. Dauxois and M. Peyrard, Phys. Rev. Lett. **70**, 3935 (1993).

[19]A. M. Kosevich and A. S. Kovalev, Zh. Eksp. Teor. Fiz. **67**, 1793 (1974) [Sov. Phys. JETP **40**, 891 (1974)].

[20]Until very recently, we were unaware that these solutions had been obtained in a brief paper by Dolgov (Ref. 1), before they were obtained independently in Refs. 2 and 4. The Dolgov paper has gone unnoticed by subsequent workers.

[21]The relevant anharmonicity parameter here is Λ_4, defined just below Eq. (3).

[22]O. A. Chubykalo, A. S. Kovalev, and O. V. Usatenko, Phys. Lett. A **178**, 129 (1993); A. S. Kovalev, O. V. Usatenko, and O. A. Chubykalo, Fiz. Tverd. Tela (St. Petersburg) **35**, 693 (1993) [Phys. Solid State **35**, 356 (1993)].

[23]S. Takeno and K. Hori, J. Phys. Soc. Jpn. **60**, 947 (1991).

[24]S. R. Bickham, S. A. Kiselev, and A. J. Sievers, Phys. Rev. B **47**, 14 206 (1993).

[25]S. A. Kiselev, S. R. Bickham, and A. J. Sievers, Phys. Rev. B **48**, 13 508 (1993).

[26]P. F. Byrd and M. D. Friedman, *Handbook of Elliptic Integrals for Engineers and Physicists* (Springer-Verlag, Berlin, 1954).

[27]S. R. Bickham, A. J. Sievers, and S. Takeno, Phys. Rev. B **45**, 10 344 (1992).

[28]As we have pointed out, the restrictions imposed by the RWA time-average method upon the time dependence of the ZBM perturbations indicate that the physically meaningful solutions to Eq. (21) should satisfy $|\lambda/\omega|\ll 1$. This might seem to suggest that in our derivation of the ZBM stability equations, we could have neglected the second time derivative terms $\ddot{\xi}_n$, $\ddot{\phi}_n$, and $\ddot{\Delta}_n$ occurring in the left-hand side of Eqs. (4)–(6), compared with the first derivative terms such as $2\omega\dot{\xi}_n$. In fact, such an approximation was used to determine

the (k_2,k_4) ZBM stability equations in Ref. 16. Unfortunately, the importance of the first and second derivative terms also depends upon the relative magnitudes of ξ_n, ϕ_n, and Δ_n. Hence, in the absence of *a priori* information about ξ_n, ϕ_n, and Δ_n, these second derivative terms must be retained. Indeed, we have found that the growth rates predicted by Eq. (21) are substantially different from the rates predicted when the second time derivative terms are neglected, and the inclusion of such terms is essential for producing growth rates in good agreement with our MD simulations.

[29]N. Budinsky and T. Bountis, Physica D **8**, 445 (1983).

[30]See, for instance, M. P. Allen and D. J. Tildesley, *Computer Simulations of Liquids* (Clarendon, Oxford, 1987).

[31]For (k_2,k_3,k_4) obtained from a Lennard-Jones potential, the occurrence of the double minimum requires an increase in the interparticle separation that is 8% beyond the minimum energy equilibrium value. For comparison, a typical change in the lattice constant due to thermal expansion for simple materials is roughly 3% between absolute zero and the melting point (Ref. 38). The double minimum occurs at even larger fractional lattice constant increases for the other two potentials, Morse and Born-Mayer, considered in this paper. Note that the above double-minimum criterion is for a (k_2,k_3,k_4) expansion of the two-particle potential and does not include the effects (typically small) due to multiple particles in a lattice.

[32]To see that the $k_3>0$ results can be generated from the $k_3\leq 0$ results, we note that the ILM equations (7) and (8) and ZBM stability equations (15)–(20) are invariant under the substitutions $k_3\rightarrow -k_3$ and $\Delta_n\rightarrow -\Delta_n$. Thus, for fixed values of k_2, k_4, and the amplitude, the $\pm k_3$ ILM and ZBM frequencies and dynamical displacements are the unchanged, whereas the static displacements change sign. Moreover, our predicted ZBM instability growth rates remain unchanged under these transformations. Hence all of our ZBM instability perturbation growth rate and ILM frequency plots would remain unchanged if we replaced k_3 with $-k_3$.

[33]W. Magnus and S. Winkler, *Hill's Equation* (Interscience, New York, 1966); C. Hayashi, *Nonlinear Oscillations in Physical Systems* (McGraw-Hill, New York, 1964).

[34]Y. A. Kosevich, Phys. Rev. Lett. **71**, 2058 (1993).

[35]It is interesting to note that repeating these MD simulations, but using *finite* seed perturbation amplitudes that are 1% of the unperturbed mode amplitude, reveals that the vertical width of the stable region in Fig. 14 decreases by a small amount. A spot check at four representative values of Λ_3 shows that upper (ILM-related) instability boundary of this figure moves down by less than 1% of vertical width of the stable region, while the lower boundary moves up between 3% and 7%. MD simulations using smaller perturbations show that this small smearing out of the stability region boundaries is a real finite perturbation effect and is *not* due to any failure of the Floquet stability analysis for infinitesimal perturbations.

[36]A. Rosenberg, C. E. Mungan, A. J. Sievers, K. W. Sandusky, and J. B. Page, Phys. Rev. B **46**, 11 507 (1992).

[37]D. F. Eggers, Jr., N. W. Gregory, G. D. Halsey, Jr., and B. S. Rabinovitch, *Physical Chemistry* (Wiley, New York, 1964).

[38]*Thermophysical Properties of Matter,* TRRC Data Series Vol. 13, edited by Y. S. Touloukian (IFI/Plenum, New York, 1977).

[39]J. Pouget, M. Remoissenet, and J. M. Tamga, Phys. Rev. B **47**, 14 866 (1993).

[40]C. Jaffé and P. Brumer, J. Chem. Phys. **73**, 5646 (1980).